We would like to thank Referee # 1 for the detailed comments, useful suggestions and illustrative figures. The paper has been revised according to the referee's comments and suggestions. The revised texts are highlighted in the paper. One subsection about the wavelength dependence of actinic flux has been added in Section 3 with one new figure, Fig. 2. A picture of the instrument has been included as Fig. 1. Some references have been included.

All the questions are in *Italic* font, the answers are in blue normal font.

Interactive comment on "Analysis of actinic flux profiles measured from an ozone sonde balloon"

by P. Wang et al.

Anonymous Referee #1

Received and published: 5 January 2015

The actinic flux drives the photochemistry of the atmosphere. As such its behaviour and understanding of the processes that affect it, is of great importance. Surprisingly there are very few measurements of this quantity under varying atmospheric conditions. The work presented in this paper describes a new instrument that have the potential to greatly improve this lack of measurements of this important quantity. It may be noted that an equally important radiative quantity, the net radiative heating/cooling rate that drives the atmospheric circulation, is on an even worse footing when it comes to atmospheric profile measurements.

Considering that the instrument is uncalibrated the authors are able to obtain a lot of useful insight by including ancillary satellite and ground-based information in their analysis. The main weakness of the paper is the assumptions used in the radiative transfer modelling. A single wavelength is used to represent the broad-band response of the diode detector. This may have implications for the model/measurement comparison as shown below for Fig. 11d. Also the use of a single layer cloud sometimes precludes a deeper understanding of the measurements, see remarks about Fig. 7d below. The authors are encouraged to redo the model simulations with the improvements suggested below before final publication of the manuscript.

A: The single layer cloud was chosen to limit the number of free parameters because there are no multi-layer cloud products from the SEVIRI CPP algorithm. We have added a subsection on the wavelength dependence of the actinic flux (Sect. 3.2). In Sect. 3.2 actinic fluxes have been simulated at 5 wavelengths from 450 to 650 nm. The question about Fig. 11d has been replied in the specific remarks.

Specific remarks

- *Page 31171, line 4: It is stated that actinic flux profiles have been measured by tethered balloons and aircrafts. It might also be mentioned that actinic flux relevant radiation profiles have been measured by balloons in the stratosphere (Schiller et al, 1994) and the troposphere and stratosphere (Kylling et al., 2003). Furthermore, accurate spectral actinic flux measurements were made by Hofzumahaus et al., 2002.*

A: The references have been included in the introduction.

• Page 31171, lines 23-24: The Junkermann (1994) and Palancar et al. (2011) papers are mentioned, but the results they obtained are not summarised as is done for the other cited papers. For completeness please also do so for these two references.

A: The results from these two references are summarized and included in the introduction section.

• Page 31172, lines 4-20: The wavelength dependence of the actinic flux should be further emphasized. The vertical profile of the actinic fluxes relevant for ozone and nitrogen dioxide are very different due to the processes that affect them. This should be discussed in connection to what the diode instrument measures.

A: Thank you for the suggestion. The text in the introduction has been revised. The simulation of actinic fluxes at different wavelengths has been added to Sect. 3.

• Page 31172, lines 21-28: It might be mentioned that the CMF is wavelength dependent as demonstrated by Seckmeyer et al. (1996).

A: The wavelength dependence of CMF has been included in the text now.

• Page 31172, line 24: It is stated that the CMF is the "ratio between UV radiation ...". Clearly the CMF is not restricted to UV radiation. Please remove "UV" from the sentence.

A: 'UV' has been removed.

• Page 31173, line 5: A plot showing the spectral response of the diode should be included. This is important documentation of the instrument and makes it easier to understand what it is actually measuring. See also comments to Fig. 11d below.

A: We did not measure the spectral response of the diode, because we do not have the equipment to do this. The LED used in this paper is similar to the Radio Shack green LED, which spectral response is shown in Fig. 2 of Brooks and Mims (2001). The spectral response covers the range from 450 nm to 580 nm and is asymmetric. The peak of the response function is at about 560 nm whereas the middle of the response function is close to 525 nm. This has been discussed in the revised paper.

Brooks, D. R., and F. M. Mims III (2001), Development of an inexpensive handheld LED-based Sun photometer for the GLOBE program, J. Geophys. Res., 106(D5), 4733–4740, doi:10.1029/2000JD900545.

• Page 31173, lines 5-27: Please include following information:

– If you measured the angular response of the instrument, please include plot.

– A picture showing the instrument would be helpful.

– What is the temporal sampling frequency?

– Where in the balloon payload is the instrument located? Please discuss possible effects of shadow from the balloon and/or the payload.

A: A picture of the instrument has been added as Fig. 1. The temporal sampling is 1 second, but the data are averaged over 10 seconds. The ozone sonde is attached to the balloon using a line of 15-20 meters long and the light sensor is located at 2 m below the ozone sonde.

Since the ozone sonde is connected to the balloon using a long line of 15-20 meters, we do not expect that the shadow of the balloon affects the light sensor measurements. Furthermore, the solar zenith angle (SZA) is usually larger than 30 deg during the measurements, so the shadow of the balloon would not be directly below the balloon. However, in case SZA < 30 deg, at high altitudes (~30 km) the light sensor went sometimes into the shadow of the balloon for a few seconds, because of the rotation (swing) of the light sensor below the balloon. These data points have been identified and removed already.

This information has been added to the text in Sect.2.

The angular response of the instrument has been checked before launch and was adjusted to within 2%. The small scale variations of the measurements above cloud top and clear-sky cases are smaller than 2%. This suggests that the angular response of the instrument is <2% during the measurements.

• Page 31174, lines 12-25: Which ozone cross section and Rayleigh scattering cross section were used?

A: ozone cross section is taken from Johnston (1997).

H.S. Johnston, personal communication (1997) to E.-P. Röth, R. Ruhnke, G. Moortgat, R. Meller, and W. Schneider, Berichte des Forschungszentums Jülich, jül-3340, 1997. (http://satellite.mpic.de/spectral_atlas/cross_sections/Ozone/O3_Johnston(1997)_298K_408-599nm.txt)

Rayleigh scattering cross section is from Bodhaine et al., 1999.

Bodhaine, B.A., N.B. Wood, E.G. Dutton, and J.R. Slusser, On Rayleigh Optical Depth Calculations, J. Atmospheric and Oceanic Technology, vol. 16, 1854-1861, 1999.
The references have been included in the paper and the text has been included in Sect. 3.

• Page 31174, line 21: What is the justification for using a single wavelength in the radiative transfer modelling and not doing it correctly by calculating a spectrum and convolving the spectrum with the spectral response of the diode? See also comments to Fig. 11d below.

A: The reason for the approximation of using a single wavelength is that the scattering by clouds has hardly any wavelength dependence in the visible wavelength range. Furthermore, the wavelength dependence of Rayleigh scattering has less influence in the visible range than in the UV range. Another reason is that we do not have to simulate the absolute value of the actinic fluxes. The approximation of using a single wavelength is mostly valid for simulations at small solar zenith angles, say SZA < 45 deg. At large solar zenith angles (SZA > 60 deg), indeed a spectrum has to be simulated and convolved with the spectral response of the LED.

Simulations of actinic flux profiles at different wavelengths have been included in Sect. 3 in the revised paper.

• *Page 31175, line 9: is the 3 km x 6 km SEVIRI resolution latitude longitude or vice versa?*

A: Longitude x latitude. The sentence has been revised.

• *Page 31176, line 15: The albedo used in 1D radiative transfer models is an effective albedo. As the altitude of the instrument increases the effective albedo "seen" by the instrument will change as the instrument "sees" a larger and larger area including the ocean to the west. While the effect is probably minor due to the low surface albedo, it might be worthwhile to mention.*

A: The text has been revised.

• *Page 31177, line 24: How was it determined that the sky was clear? Are contrails allowed in clear-sky profiles?*

A: The clear-sky was checked from the MODIS images and Total Sky Imager data at Cabauw. Contrails may be exist.

• *Page 31177, line 24, Fig. 2a and Fig. 3: The clear-sky actinic flux profiles have some periodic small scale variability. This may be caused by rotation of the balloon and hence the payload. It might be interesting to calculate the frequency of this variability in the actinic flux and see if it is consistent with the expected period for rotation of the payload. The periodic variability in the actinic flux should be larger when the instrument is exposed to the direct sun and less or absent when the instrument is inside a cloud. This is so because imperfections in the angular response are more evident in an inhomogeneous light field. Evidence for this behaviour is seen in Figs. 3a-e where little or no small-scale variability is seen inside and below the cloud and then it appears ones the instrument is above the cloud and exposed to the direct sun.*

A: Thank you for this suggestion.

There are two possible rotations in our sonde system.

One is the swinging of the sonde below the balloon. This is considered to be a good thing, because it will keep the sensors out of the wake of the balloon, and so the potential of interference of the balloon on the temperature, humidity and ozone measurements is reduced. As the balloon is obscuring different parts of the sky, an effect on the radiation field is likely. The period of this swing is estimated to be between 10 and 20 seconds.

The other rotation of the system - including the light sensor - is spinning along a vertical axis. In 2006 and 2007 we used a line made of a twisted natural fiber. Untwisting of the line during the flight is quite likely, although we have never seen it happen. We hope and think this spinning does not affect any of our sensors.

We estimated the small scale variations using the data between 15 and 30 km in the ascending profiles. Of the 63 profile measurements, 59 have variations smaller than 2%. Based on the uniform response test before launch, the angular dependence of the instrument is as expected.

The text in Sect. 4.2 has been revised accordingly.

• *Page 31177, lines 11-12: May also sub-visible cirrus and far away clouds contribute here?*

A: Indeed there could be a contribution from sub-visible cirrus and small scale clouds. Text has been revised according.

• *Page 31177, lines 21-22: It is stated that the "altitude dependence of the internal radiation field in a scattering atmosphere depends mainly on the optical depth". It is not defined what is meant by "internal radiation". Also, depending on the wavelength, altitude distribution of the optical thickness and the magnitude of the optical depth, the amount of overlying atmosphere and its properties, possible pollution in the cloud (single scattering albedo smaller than 1.0) and surface albedo may play a role. The phase function may also be of importance depending on the phase of the cloud. Thus, this sentence appears to oversimplify as it stands. Finally, the expression within the parenthesis may be omitted. It is trivial that " = 0 at TOA.." etc.*

A: Thanks for these suggestions. The text has been revised.

• *Page 31180, line 25: Please state what the magnitude of the SEVIRI COT negative bias is.*

A: The COT retrieval error is about 15% according to the MSG CPP product description. We do not know the magnitude of the SEVIRI COT negative bias because of the small number of data used in the paper.

• *Page 31183, lines 6-8: It is stated that "COT values in the maps are averaged over 0.1 degree grids, while the COT values are given for single pixels". But in the caption of Fig. 7c the single pixel values are from 0.1 x 0.1 pixels. Are there two types of 0.1 degree pixel values? What are they and what are the differences? Please clarify.*

A: The grid is always 0.1x0.1 degree. Within the grid box, there are about 5 SEVIRI pixels. Two types of COT values are used here: one is the mean of the ~5 COT in the 0.1x0.1 degree grid box, which is used for the images. the other is the COT value of every SEVIRI pixel in the grid box, not averaged, which is used in the simulations. It has been clarified in the revised paper.

• *Page 31183, line 17: It is straightforward with a radiative transfer model to include several cloud layers and this should be done to better reproduce the measurements. In Fig. 1 (this review) single cloud layer (red) and two cloud layers (green) simulations are included. The total optical depth was 25 in both cases and the solar zenith angle as in Fig. 7d. The wavelength is 550 nm, the surface albedo 0.15 and no aerosols were included. Clearly the two layers simulation better resembles the measurements in Fig. 7d.*

The really intriguing feature with the measurements shown in Fig. 7d is the decrease in radiation as the altitude increase from about 0.5 to 2.0 km, that is between the two cloud layers. Below a sufficiently thick cloud little of no vertical variation is expected as shown by the model results in Fig. 1 (this review), green line. The behaviour of the measurements in this altitude range is unexpected. Aerosols may play a role, but it is not at all clear to this referee what the reason is for this behaviour.

A: Thank you for the simulations. We have also done simulations using two cloud layers for this case but did not show them. The result is very similar to figure 1 in this comment: we cannot simulate the decrease in the radiation when the balloon rises from 0.5 to 2.0 km altitude. It could be due to the assumed horizontal homogeneity of the two cloud layers in the simulation. It is possible that the balloon went through one cloud layer first, with no second cloud layer above, then moved into the second cloud layer after a horizontal drift below the second cloud layer.

• *Page 31184, line 18: Should it be 0.1-degree box instead of 1-degree?*

A: It should be 0.1-degree.

• *Page 31184, lines 21-22: It is stated the balloon passed through the cloud top resulting in a sharp peak in the actinic flux at 3 km. In the next sentence it is stated that the "COT increased again at about 4 km". But then the balloon was above the cloud? Or was there another cloud? Or was the ballon flying at 4 km and the COT of the underlying cloud increased? Please clarify.*

A: It was the balloon flying at 4 km and the COT of the underlying cloud increased. This has been clarified in the revised paper.

• *Page 31184, line 24: The measured and simulated profiles are said to follow each other "very well". May you please quantify "very well" by providing rms differences or similar?*

A: We have revised the text. The rms difference is difficult to quantify.

• *Page 31184, lines 25-26: Please prove your conclusion by varying the extinction coefficient with altitude and thus make the simulated actinic flux agree with the measurements.*

A: The text has been revised. We did not do extra simulations for this comment.

• *Page 31185, line 5: What is meant by "properly simulated"?*

A: The sentence has been revised.

• *Page 31185, lines 6-23: For large solar zenith angles a difference between the measured and simulated actinic flux is seen below about 10 km in Fig. 11d. It is speculated that full spherical geometry is needed to explain this discrepancy. However, the DAK simulations are made for the single wavelength of 550 nm under the assumption that this single wavelength best describes the broad band response of the diode. This assumption may hold for small solar zenith angles, but not necessarily for large solar zenith angles. The clear-sky actinic flux varies with wavelength (Rayleigh scattering). To investigate this effect the actinic flux was calculated as a function of altitude for wavelengths of 450, 550 and 650 nm for a solar zenith angle of 75 degree. A water cloud with optical thickness of 30 evenly distributed between 0.1 and 1.0 km, was included in the simulations. Pseudo-spherical geometry was assumed. In Fig. 2 (this review) the actinic flux normalised to its value at 30 km is shown for the three wavelenghts. It is seen that the actinic flux varies considerably with wavelength below about 15 km and that a wavelength of 650 nm resonably well resembles the measurement presented in Fig. 11d. Thus the choice of 550 nm in the DAK simulations is not representative for large solar zenith angles. This example very clearly demonstrates the danger involved when using a single wavelength to simulate an instrument with a broad spectral response. Rather then using a single wavelength, the DAK simulations should be made for all wavelengths covered by the diode and the resulting spectrum convolved with the spectral response of the diode.*

Finally note the difference between the black and green lines in Fig. 2 (this review). For the green (black) line the cloud optical depth was evenly distributed between 0.1 (0.8) and 1.0 km. The black line best reproduces the red line in Fig. 11d of the manuscript, but it is not clear from the text how the vertical distribution of the optical depth was for the calculation presented in the manuscript.

A: Thank you for the simulations and figure. Indeed the simulation at 650 nm fits the measurements better. However, we doubt that the green LED has much sensitivity at 650 nm, looking at the spectral data from Brooks and Mims (2001). We agree that the wavelength dependence of the AF simulation is important. Some simulations have now been included in Sect. 3 to show the wavelength dependence of AF. We agree that the wavelength dependence of the actinic flux may be the main reason for the difference between the measured and simulated actinic fluxes for this case. The simulation may not have significant improvement if a full spherical model is used. The text has been changed accordingly in the revised paper.

Fig. 2 in revised paper, Simulated actinic flux profiles at wavelengths: 450, 500, 550, 600, 650 nm at SZA = 30 and 75 degree. The cloud top is at 1.3 km, cloud base is at 0.8 km, cloud optical thickness is 30. The aerosol optical thickness is 0.18 at 550 nm and surface albedo is 0.15. The normalized actinic fluxes are shifted 1 km up in the y-axis.

• *Page 31187, line 5: After the simulations have been redone accounting for the spectral response of* *the diode instrument, the shapes of measured and simulated actinic fluxes will most likely agree for SZA > 75 degree and the conclusions may be changed accordingly.*

A: We agree that at SZA > 75 deg the AF wavelength dependence is more important than at smaller SZA. Because we do not have actual spectral response measurements of our LED we are not sure whether the simulation at 650 nm would be suitable for our instrument. We have added a remark on this point.

• *Page 31194, Fig. 4a-b: Have you tried to use log-scale on both the x- and y-axes in Fig. 4a? And have you tried to use log-scale on the x-axis of Fig. 4B?*

A: Thank you for the suggestions. A log-scale for the x-axis is now used in Fig. 4b. In Fig. 4a the y-axis has been changed to Actinic flux ratio of cloud base and top.

• *Page 31195, Fig. 5a-b: Please mark the launch site in Fig. 5a or even better include a square marking the region shown in Fig. 5b. Fig. 5a looks like a MODIS image obtained directly from the MODIS web site. A little more work is warranted to make the presentation clearer.*

A: Fig. 5 has now been remade using MODIS data at 0.15x0.3 degree grid with the flight track on top of it. The white area indicates missing AOD data, this could be due to clouds.

• *Page 31195, Fig. 5c: It is not marked which lines correspond to the measurement and the model. Also, it would be interesting to include a model/measurement ratio or difference plot.*

A: The legend has been added to the figure.

Technical remarks

• *Page 31172, line 12: The sentence "the photodissociation of nitrogen ...." is unclear, please rewrite.*

• *Page 31175, lines 12-18: The sentences in this part are hard to read; please rewrite.*

A: The sentences have been rewritten.

• *Page 31186, line 15: Replace "an large" with "a large".*

A: Corrected

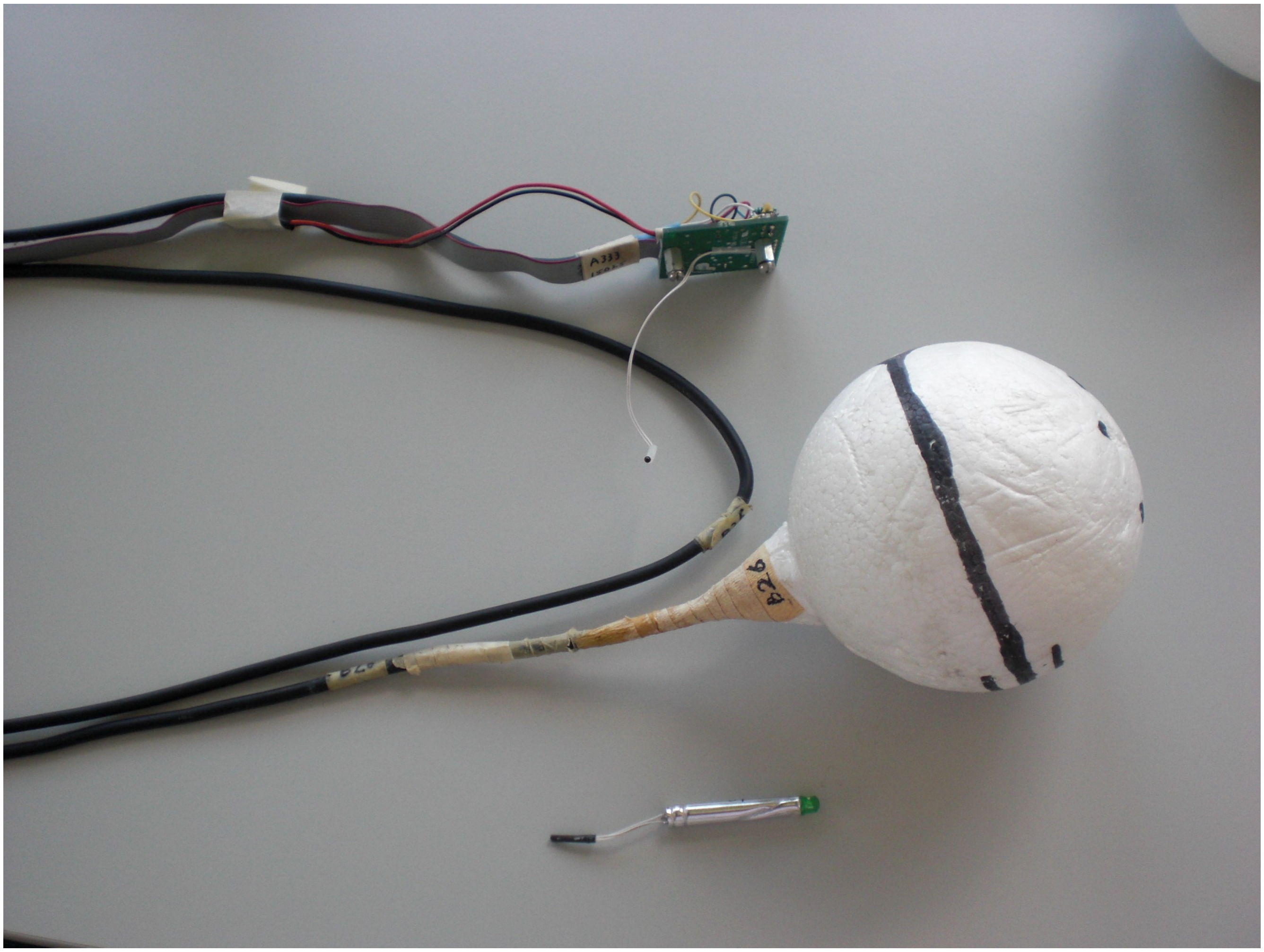

Fig.1 Photo of the light sensor: (a) data transmitter, (b) sphere, (c) green LED.

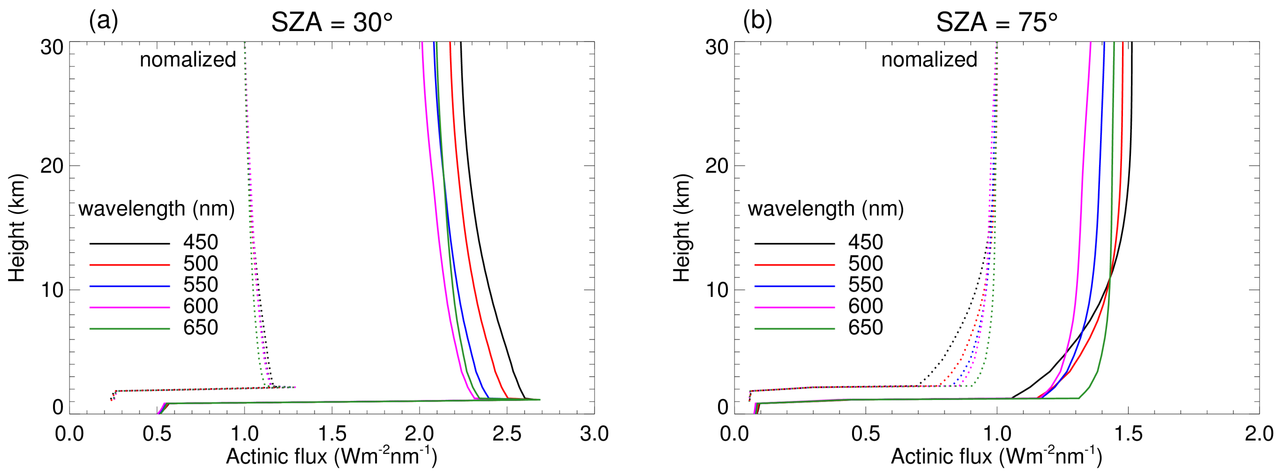

Fig. 2 Simulated actinic flux profiles at wavelengths: 450, 500, 550, 600, 650 nm at SZA = (a) 30 and (b) 75 degree. The cloud top is at 1.3 km, cloud base is at 0.8 km, cloud optical thickness is 30. Particle size of the water clouds is 10 micron. The aerosol optical thickness is 0.18 at 550 nm and surface albedo is 0.15. At every wavelength the normalized actinic flux profile is the simulated actinic flux profile divided by the actinic flux at 30 km. The normalized actinic fluxes are shifted 1 km up in the y-axis.

We would like to thank Referee # 2 for detailed comments and suggestions. The paper has been revised according to the referee's comments and suggestions. The revised texts are highlighted in the paper. One subsection about the wavelength dependence of actinic flux has been added in Section 3 (with 1 new figure). We have cited some references in the discussion of the cloud effect on AF. Three figures are added in the revised paper. A picture of the instrument has been included as Fig. 1. The wavelength dependence of the actinic flux is analyzed and presented in Fig. 2. The simulated CMF(z) has been plotted for cloudy cases in Fig. 14.

All the questions are in *Italic* font, the answers are in blue normal font.

Interactive comment on "Analysis of actinic flux profiles measured from an ozone sonde balloon"

by P. Wang et al.

Anonymous Referee #2

Received and published: 7 January 2015

Actinic flux (AF) is fundamental to atmospheric chemistry, but is highly variable and therefore difficult to quantify, particularly in the presence of clouds. Instruments for accurate AF measurements have been developed but can be expensive and difficult to operate, especially chemical actinometers. The basic concept of the paper, to build and deploy a simple AF instrument with ozone sondes and thus obtain frequent vertical profiles, is excellent. True, this is at green wavelengths that are not the most relevant for photolysis (UV wavelengths would be more relevant), but even so it is a very good test for radiative transfer models in the presence of clouds, and confidence at green wavelengths increases confidence at UV wavelengths. Another strength of the paper is the analysis of cloud data from satellites, to help understand what the detector actually saw during the flights. Temporal and horizontal changes in cloud optical thickness have to be considered, and the authors did a nice job with that.

There are however a few issues that should be addressed to improve the manuscript. ISSUE 1: The general discussion of cloud effects on actinic radiation is weak theoretically. There is quite a bit of literature on these effects, and while the authors cite some of the key papers, they don't use content from those papers to help them interpret their own results. This leads to assertions that are not true, or not relevant, or misleading.

Specific points needing improvement:

31175/19-21: The peak AF is not at cloud top, but usually below that. For very thick clouds, the peak is barely below cloud top, but for thinner clouds the peak could be at the midpoint between cloud top and bottom, and even closer to cloud bottom if the surface albedo is high (e.g. over snow). So it is incorrect to automatically place model cloud tops at the same height as the peak measured AF. Since the comparison to the model is only rough, it really does not make much difference, except that it propagates a wrong conceptual understanding.

A: Thank you for the comments. We agree with the point raised. The location of peak AF in clouds has been clarified in the revised paper. The texts have been revised to avoid misunderstanding.

Figure 1b and text p.31177/5-15: The correlation between AF and irradiance is in general non-linear, as it depends on the diffuse/direct ratio and therefore on the presence/absence of the direct solar beam. So seeing a quasi-linear correlation only says that the scatter is too large to detect the non-linearity, and is not a confirmation of accuracy.

A: The text in Sect. 4.1 has been revised according to your comments.

31178/25: While multiple scattering helps to increase the AF, it is not required. Single scattering alone can do that.

A: The texts have been revised according to your comment.

31178/28-39 to 31179/1-3: This is not limited to isotropic scattering, and was earlier shown to occur by Madronich (1987, cited but not used). The exact value of mu_0 depends on the directional distribution of the diffuse radiance, limiting to 0.5 (cos 60deg) for isotropic light but mu_0 = 1/sqrt(3) (cos 52 deg) in the commonly used delta-Eddington approximation. The authors are mixing some of these concepts in lines 31179/1-10.

A: The text has been revised. We have used Madronich 1987 to explain the impact of clouds on actinic fluxes in Sect. 4.5.

31180/15-17: Enhancements of surface actinic flux in the presence of broken clouds have been measured and explained in earlier work, e.g. Lantz et al. (JGR,101,14693,1996) for JNO2, Crawford et al. (JGR, doi:10.1029/2002JD002731) for spectrally resolved AF, and these should be cited here.

A: The references have been included.

31180/18: Again multiple scattering helps, but is not required to cause enhancement. Single scattering would suffice, depending on the COT. For thin clouds, single backscattering probably dominates over multiple scattering. Also, this backscattering can occur not only at cloud top but throughout the cloud.

A: The texts have been revised according to your comments.

31185/8-10: How do you know that you are really testing the pseudospherical part of the code? What is the air mass correction factor (as a function of altitude) at 78 degrees, compared to simple secant(sza)? How much worse would the agreement be, if you used only plane-parallel?

A: In the DAK code, the pseudo-spherical part and plan parallel part use different subroutines. We have found that the disagreement between DAK simulated and measured actinic fluxes at SZA of 78 degree may come from the wavelength dependence of AF. The pseudo-spherical correction seems less important here. The discussion has been revised.

31185/22-23: It is not surprising that increasing COT makes little difference at low sun, high altitude. In these conditions, the direct solar beam dominates. Reflected radiance is proportional to cos(sza), so even if clouds reflected 100% of the incident radiation, the contribution to the AF is much smaller than that from the direct beam. Furthermore, increasing cloud optical depth from a large value (say 50) to even larger values (100, or 1000) makes only small changes to cloud reflectivity because it is already close to 100%. That is why it does not help much to increase the COT. It seems premature to invoke the need for fully spherical calculation based on this result.

A: Thanks for the comment. The text has been revised accordingly.

31186/16: The enhancements near cloud top are larger than above the cloud only for high sun (small sza). The opposite occurs for low sun, as also seen in Fig. 11, and as already discussed above (changing sign at 52 or 60 deg, depending on approximation).

A: Thanks for the comment. It has been included in Sect. 3 to explain the simulated actinic fluxes at SZA of 30 and 75 degree.

31187/6: Vertical position is also extremely important, as shown in Fig. 7: A factor of two error is seen in the model because it does not have the low clouds. Note that these errors are largest in the lower atmosphere, which is where AF is most relevant to air quality (NO2/O3 ratios, etc.). So while the altitude range of error seems small, it is a most important part.

A: We agree with your comment. We realized that it would be better to show the simulations of Fig. 7 with two cloud layers. However, we do not know the COT of each cloud layer and how the two layers are overlapping. We have tried to set two cloud layers in DAK. Then the simulated AF between the two cloud layers improves but does not really match the measurements. Therefore we did not change this figure.

ISSUE 2: Normalizations, and showing the effect of clouds. The several normalizations performed (model/observation, clear/cloudy) cause loss of useful information. I understand that the green AF detector is uncalibrated, and sometimes changes even between flights. That is ok. But the model IS calibrated (quite well, based on Fig. 6), and could produce results in units of AF, for example photons cm-2 s-1 nm-1. At the very least, the model can produce AF relative to clear sky, i.e., CMF(z). Figures 7-11(d) show the vertical profiles of AF from the model and the observations, both normalized to 1.00 at 30 km, but this should not be confused with the CFM(z). It would be interesting to plot also CMF(z) (obviously from the model, as this is not available from the measurement). This could be an additional curve on the same plot (the numbers should be similar although a bit larger). For example, in Fig. 8d, the peak AF (at about 1.5km) is 2.0 x the value at 30 km. But the value at 30 km is also larger than clear sky (because of cloud reflection from below), so the actual CMF peak at 1.5km is larger than 2.0, perhaps as high as 3.0. In other words, normalizing both model and observations to 1.00 at 30 km *causes loss of information about the CMF(z). Because of this excessive normalization, the manuscript doesn't show CMF(z), one of the original objectives of the work. (Figure 4 does show CMF at cloud base and cloud top, but with much scatter - see below).*

A: Thank you for the useful suggestion. We have now added a new figure, Figure 14, to show the simulated CMF(z) for the cloudy cases. Furthermore, in Fig. 2 the simulated AF is also shown in W/m2/nm, assuming the incident solar flux is 1 W/m2/nm. So in this way the information content on absolute AF values is maintained.

OTHER MINOR ISSUES

31172/21-23: Palancar et al. 2011 also presented most of their results in terms of the CMF statistics, based on thousands of UV observations from aircraft. How do CMFs in the present work compare with those of the earlier study?

A: It is hard to compare the CMFs in this paper with those of Palancar et al. (2011) because of the different wavelength range: Palancar uses broadband actinic flux integrated from 298 to 422 nm, whereas we use a green LED and the simulations have been done at 550 nm.

Figure 2: Difficult to see. Most of the discussion (p. 31178) is for 0-5 km so I suggest showing only 0-5 km, or at most 0-6 km in the plot, since you in any case dismiss values above 5 km as being due to unknown changes in AOT and surface albedo. (But later you normalize to values at 30 km, so this argument is not being applied consistently).

A: The aim of Fig. 2 is to show the original measurements. The normalization is used when the model and measurement are compared.

Figure 4a: Strange to plot ratio of top/base vs. ground irradiance. Why not plot the reciprocal, base/top vs. ground irradiance? It should be close to a simple straight line through zero, rather than this unnecessary hyperbolic-looking function. This was done in Fig. 6 for global irradiance, and it looks nice there.

A: Thank you for the suggestion. The plot has now been changed into base/top vs. ground irradiance.

Figure 4b: why such a large scatter when there are no clouds? Agreement for clear sky should be better, CMF = 1.00.

A: The COT is taken from SEVIRI data at the pixel size of 3x6 km2. It is possible that small and local clouds, which have not been detected by SEVIRI, impacted the AF measurements. The figure has been changed into logarithm x-axis now.

31180/20: The figure contradicts the text, that cloud top CMF is more sensitive to sza. For example, at COT = 40, CMF at cloud base decreases by a factor of 2 (as sza goes from 30 to 60) while CMF at cloud top only decreases by 30%.

A: The text has been revised.

31180/25: This makes no sense. How can you get such large CMF (2 or more) for very low COT? How large a bias in COT do you need to gain a factor of 2 in the CMF? Judging from your model curves, you would need COT 30 to get CMF 2, instead of COT 0. This is a very large bias. Please clarify.

A: The SEVIRI COT may not be representative for the clouds that impacted the AF measurements at very small COT values or very local clouds. It may show up as large CMF at small COTs. This has been clarified in the revised paper.

31184/10 and Fig. 8: it would be interesting to see the model results BEFORE the ad hoc COT reduction from 30 to 20. Otherwise the logic becomes circular: if measured COT has to be changed to get agreement with modeled actinic flux, then there is no closure.

A: The actinic flux calculated using COT = 30 is larger than that using COT =20 between 15 and 34 km. If COT = 30, after normalization, the actinic flux profiles have less agreement below 10 km. Since the COT is rather variable in the SEVIRI images, there are often mis-matching in time or geolocation between the SEVIRI and the balloon measurements. At high altitude, the actinic flux can be affected by clouds from a larger area, not just the clouds below the balloon. This may cause more uncertain in selecting the right COT in the actinic flux simulations. It might be the reason that we often have to modify the COT when balloon is at high altitude to get a better closure.

31186/14: an -> a

A: Corrected.

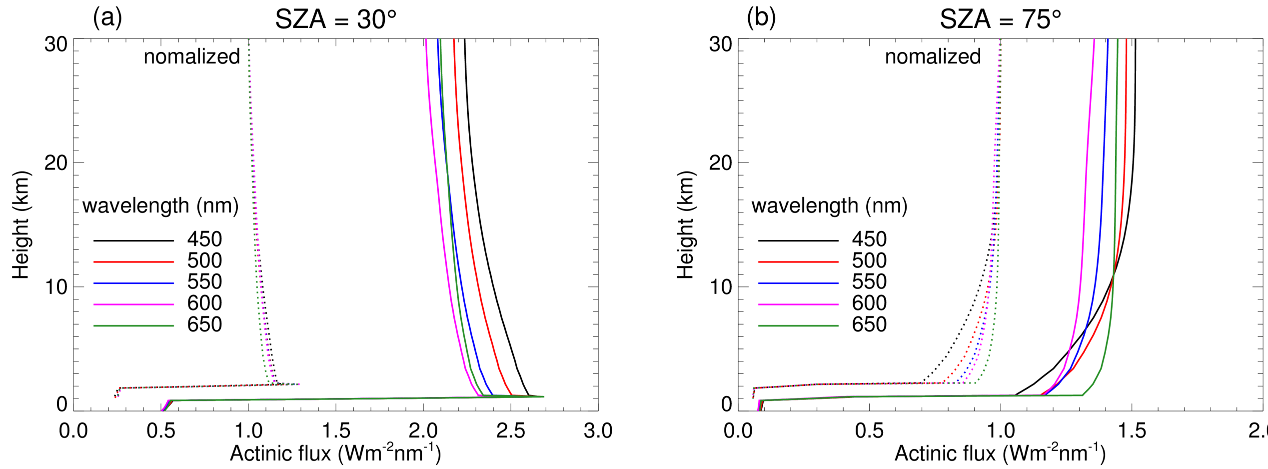

Fig. 2 Simulated actinic flux profiles at wavelengths: 450, 500, 550, 600, 650 nm at SZA = (a) 30 and (b) 75 degree. The cloud top is at 1.3 km, cloud base is at 0.8 km, cloud optical thickness is 30. Particle size of the water clouds is 10 micron. The aerosol optical thickness is 0.18 at 550 nm and surface albedo is 0.15. At every wavelength the normalized actinic flux profile is the simulated actinic flux profile divided by the actinic flux at 30 km. The normalized actinic fluxes are shifted 1 km up in the y-axis.

\

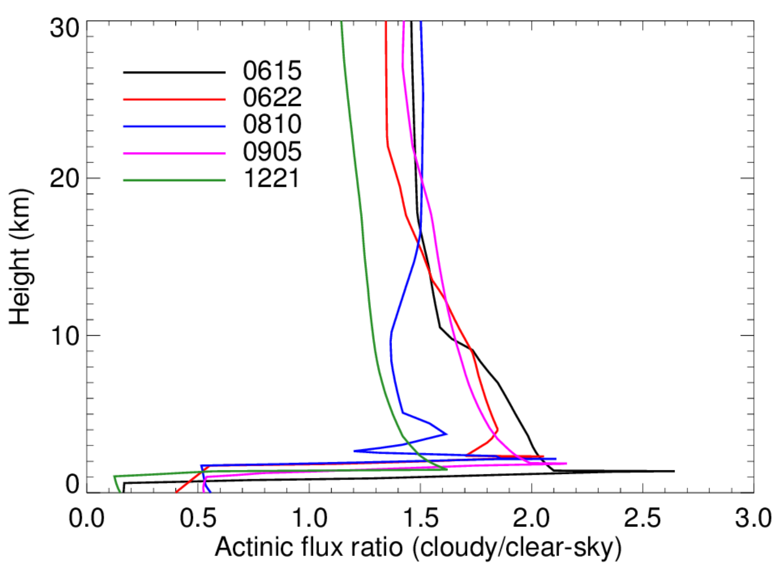

Fig. 14 Simulated actinic flux ratio (cloudy/clear-sky) for the cloudy cases in Figs. 9-13.

Manuscript prepared for Atmos. Chem. Phys. Discuss.
with version 2014/09/16 7.15 Copernicus papers of the LaTeX class copernicus.cls.
Date: 20 March 2015

Analysis of actinic flux profiles measured from an ozone sonde balloon

P. Wang, M. Allaart, W. H. Knap, and P. Stammes

Royal Netherlands Meteorological Institute (KNMI), De Bilt, the Netherlands

Correspondence to: P. Wang (ping.wang@knmi.nl)

Abstract

A green light sensor has been developed at KNMI to measure actinic flux profiles using an ozone sonde balloon. In total, 63 launches with ascending and descending profiles were performed between 2006 and 2010. The measured uncalibrated actinic flux profiles are analyzed using the Doubling Adding KNMI (DAK) radiative transfer model. Values of the cloud optical thickness (COT) along the flight track were taken from the Spinning Enhanced Visible and Infrared Imager (SEVIRI) Cloud Physical Properties (CPP) product. The impact of clouds on the actinic flux profile is evaluated on the basis of the cloud modification factor (CMF) at the cloud top and cloud base, which is the ratio between the actinic fluxes for cloudy and clear-sky scenes. The impact of clouds on the actinic flux is clearly detected: the largest enhancement occurs at the cloud top due to multiple scattering. The actinic flux decreases almost linearly from cloud top to cloud base. Above the cloud top the actinic flux also increases compared to clear-sky scenes. We find that clouds can increase the actinic flux to 2.3 times of the clear-sky value at cloud top and decrease it to about 0.05 at cloud base. The relationship between CMF and COT agrees well with DAK simulations, except for a few outliers. Good agreement is found between the DAK simulated actinic flux profiles and the observations for single layer clouds in fully overcast scenes. The instrument is suitable for operational balloon measurements because of its simplicity and low cost. It is worth to further develop the instrument and launch it together with atmospheric chemistry composition sensors.

1 Introduction

Atmospheric trace gases such as ozone and nitrogen dioxide are involved in a series of chemical reactions driven by solar radiation at UV wavelengths (Crutzen and Zimmermann, 1991). Actinic flux – which is the integral of the radiance over all directions, i.e. 4π solid angle – is relevant ~~for~~ to the process of photodissociation. Clouds have a large impact on the actinic flux in the atmosphere and, consequently, on photodissociation rates (Calbó et al., 2005). Therefore, the actinic flux profile is important for the study of the change in concentration of chemically reactive components in the atmosphere and is preferably measured together with the atmospheric chemical composition. Such actinic flux profiles have been measured by means of ~~tethered~~ balloons and aircrafts during several campaigns.

During the Atlantic Stratocumulus Experiment (ASTEX), tethered balloon soundings were ~~made~~ performed on Santa Maria, Azores. Vilà-Guerau de Arellano et al. (1994) compared measured actinic flux profiles with simulations using a delta-Eddington model. Excellent agreement was found for fully cloudy scenes. The authors reported that the actinic flux decreased from cloud top to cloud base. At cloud top the actinic flux was higher than the clear-sky actinic flux, while at cloud base the actinic flux was lower than the clear-sky values. In the First ISCCP Regional Experiment (FIRE III) Arctic Cloud Experiment actinic fluxes were measured above sea ice in May 1998. De Roode et al. (2001) found that the actinic flux profile within clouds is nearly constant with height, except in a shallow layer below cloud top where the actinic flux revealed a large increase. The authors attributed this feature to the bright surface of sea ice (high albedo). Actinic fluxes have been measured on the ground and on an aircraft during the INSPECTRO campaign to study the effect of clouds on the spectral actinic flux in East Anglia England in 2003. Kylling et al. (2005) showed that the spectral actinic flux can be reproduced with a 1-D radiative transfer model for clear-sky and fully cloudy cases. They reported that the actinic flux (in the UV wavelength range) could be enhanced by as much as 60–100 % above clouds and reduced by 55–65 % below clouds, as compared to the clear-sky situation. Junkermann (1994) measured J(O^1D) actinic flux within and above stratiform clouds and above snow surfaces from a hang glider ~~.~~ with flight altitude of up to 1 km above ground. The actinic flux showed a very strong contribution of reflected or backscattered radiation within the planetary boundary layer. Palancar et al. (2011) reported extensive comparisons between aircraft-based measurements (between 0.1–11.9 km altitude) of actinic fluxes and ~~the~~ Tropospheric Ultraviolet-Visible (TUV) model simulations. They found a good agreement between the measured and TUV clear-sky model actinic fluxes (integrated from 298 to 422 nm). Including both cloudy and clear-sky conditions, the ratio of observed actinic flux to the TUV clear-sky model value was 1.1+/-0.3. Furthermore, accurate spectral actinic flux measurements (280 - 420 nm) between ground and 12 km altitude were made by Hofzumahaus et al. (2002) from an aircraft. Actinic flux profiles have also been measured by balloons in the stratosphere (Schiller et al., 1994) and in the troposphere and stratosphere (Kylling et al., 2003).

On the ground, UV monitoring stations usually measure spectral irradiances. The relation between the actinic flux and the irradiance was studied in several papers (e.g. Madronich, 1987; van Weele et al., 1995; ~~McKenzie~~ Kazadzis et al., ~~2001; Kazadzis~~ 2000; McKenzie et al., ~~2000~~2001). In general, the actinic flux correlates well with the irradiance on the surface but the relationship depends on wavelength, surface albedo, solar zenith angle, and cloud conditions.

Most actinic flux profiles presented in the literature were measured in the lower troposphere in the UV wavelength range. Actinic flux observations at green wavelengths (about 510 nm) are more representative for photodissociation by visible light. In combination with ozone and NO_2 observations, the actinic flux profile observations are useful to investigate the photostationary state relationship between NO, NO_2 and O_3 in cloudy scenes in detail (Cantrell et al., 1993; Mannschreck et al., 2004). Knowledge of the chemical inter-relationship between O_3 and NO_2 is important to better constrain their vertical profile in air quality models and in satellite retrievals of O_3 and NO_2. ~~Although~~ The actinic flux at UV wavelengths is more relevant to the photodissociation of ~~nitrogen dioxide mainly in UV wavelength~~NO_2 and O_3 than the actinic flux at visible wavelengths. However, good measurements and simulations of the actinic flux at visible ~~wavelength~~ wavelengths will give some confidence ~~with our simulations in~~ in our simulations at the UV wavelengths. It was intended to be a cheap, disposable instrument and no harm for the environment. Therefore, we measured actinic flux profiles using a green light sensor attached to an ozone sonde. Another advantage of using an operational ozone sonde is the large altitude range (from surface up to 35 km) and the regularity of launching. The aims of the actinic flux profile measurements are to evaluate the impact of clouds on the actinic flux profiles and to better constrain the O_3 and NO_2 chemical inter-relationship in atmospheric chemistry models.

The cloud modification factor (CMF) is often used in the analysis of cloud effects on UV radiation (e.g. Seckmeyer et al., 1996; Mayer et al., 1998; Schwander et al., 2002; Antón et al., 2012; Mateos et al., 2014). The cloud modification factor is the ratio between ~~UV~~ radiation under cloudy and clear-sky conditions. The ~~UV~~ radiation for clear-sky scenes is calculated using the same atmospheric states as for cloudy scenes. ~~CMF has~~ It has been demonstrated and explained that the surface CMF in the UV has a wavelength dependence (Seckmeyer et al., 1996; Crawford et al., 2003). The transmission of clouds alone does not have a significant wavelength dependence in the UV but Rayleigh scattering does. According to Kylling et al. (1997), the observed wavelength dependence is due to photons reflected by clouds, then the photons are scattered downward by Rayleigh scattering above the clouds and transmitted through the clouds to the ground surface. CMF has been used to evaluate the cloud effects on irradiance, actinic flux and photolysis rate. We also use CMF in our analysis of the actinic flux profile at a green wavelength.

In this paper we will describe the ~~instruments~~ instrument and measurements in Sect. 2. The simulation method for the actinic flux profiles is presented in Sect. 3. The results are shown in Sect. 4. Conclusions are drawn in Sect. 5.

2 Instruments and measurements

A light sensor has been developed at KNMI using a commercial green LED (Light Emitting Diode) with a diameter of 5 mm made of Gallium-Phosphide (GaP). It is mounted in the center of a 10 cm Styropor (Polystyrene) sphere. A picture of the light sensor and sphere is shown in Fig. 1. The sphere acts both as a thermal insulation and a light diffuser. The detector and amplifier are temperature stabilized at 25 °C. The instrument has been designed to have uniform response to sunlight. The point on the sphere where the LED sensor was inserted is called north pole. The senor was glued at a position in the sphere where its sensitivity to sunlight was comparable when the sphere was lit from the north or the south pole. After the instrument was completed, it was held in a beam of sunlight that would enter a single window in an otherwise dark room. The response of the instrument was checked by rotating the sphere. If it was found to be more sensitive on one side, a black permanent marker pen was used to make marks on that side. Typically it was found that the sensitivity was higher (10 % or so) on the equator compared to the poles. This process was repeated until the response of the instrument varied less than 2 % when the sphere was rotated. So the spheres have a number of black lines around the equator to make the sensitivity uniform. The light sensor is not absolutely calibrated and the measured actinic profile is in an arbitrary unit. However, before launching a light sensor, inter-comparison measurements have been performed on the ground together with one reference light sensor which is kept and not used for launching. If the reference sensor does not change with time, the actinic flux profiles measured with different sensors should be intercomparable. The exact spectral response of the light sensor is not measured. The spectral response of the same type of sensor has been shown by Brooks and Mims (2001) in their Fig. 2 for the RadioShack green LED. The spectral response of the RadioShack green LED covers the wavelength range 450–580 nm with the peak value at about 560 nm and center at 525 nm. At present, the light sensor is mainly used to evaluate the cloud effects on actinic flux profiles. The green light sensor is chosen because it is not sensitive to ozone and water vapor absorptions, so that the impacts of clouds and aerosols on the actinic fluxes can be separated from the effects of gas absorptions.

The light sensor is launched together with the ozone sonde balloon and the data are transmitted during flight. The light sensor attached to a line and located at about 20 m below the balloon and 2 m below the ozonesonde. Because the payloads of the balloon are rotating during flight, the light sensor could rotate in the shadow of the balloon when the balloon is at high altitude and the sun is almost overhead (SZA $< 30^\circ$). This can be identified as a sharp dip in the measured actinic flux profile from the 1-second data record. The measurements impacted by the shadow of the balloon have been removed before the data are averaged over 10 s and stored. The instrument weighs about 100 gram, is low cost and can be reused after recovery. The ozone sonde is launched at 11:30 UTC on every Thursday at De Bilt (5.18° E, 52.10° N), the Netherlands. The vertical velocity of the ozone sonde is typically 5 m s^{-1} and reaches an altitude of 30–35 km in about 100 min. After the burst of the balloon the sonde drops back to the ground with a parachute in about 60 min. The data stream includes ascending and descending values of time, altitude, pressure, temperature, relative humidity, ozone partial pressure, and actinic flux. The trajectory of the balloon is obtained from GPS data.

3 Methods for the actinic flux profile simulations

3.1 Radiative transfer modelling and input data

The Doubling-Adding KNMI (DAK) radiative transfer code (De Haan et al., 1987; Stammes et al., 1989; Stammes, 2001) is used to simulate the measured actinic flux profiles. DAK is a 1-D plane-parallel radiative transfer code with a pseudo-spherical correction for solar zenith angles (SZAs) greater than 75°. Because the measurements were made at noon, the SZAs are usually smaller than 75° except in December and January. The DAK model has been used by van Weele et al. (1995) in the UV-A actinic flux calculations. The DAK simulated surface shortwave broadband irradiances have good agreement with the ground-based BSRN (Baseline Surface Radiation Network) measurements for clear-sky and overcast water clouds scenes (Wang et al., 2009, 2011). In this paper, the DAK simulations were performed for $\lambda = 550$ nm to represent the green wavelength range. Absorption by ozone is taken into account by using the shape of a climatological ozone profile and scaling it to the assimilated total ozone column at 12:00 UTC using OMI total ozone data (Eskes et al., 2003). The ozone absorption cross section is taken from Johnston (1997). Water vapor absorption is not taken into account in the simulations because it is weak at 550 nm. The Rayleigh scattering cross section is calculated according to Bodhaine et al. (1999).

For clear-sky scenes, aerosol optical thickness (AOT) data are taken from the SPUV sunphotometer at Cabauw (4.93° E, 51.97° N, 20 km SW of De Bilt) because AOT is not measured in De Bilt. For cloudy scenes, a default AOT of 0.18 at 550 nm is used, which is close to the climatological value for Cabauw. The LOWTRAN rural aerosol profile is used, with addition of a well-mixed aerosol layer from the surface to the top of the boundary layer for clear-sky scenes. The latter is determined from the lidar measurements in Cabauw.

For cloudy scenes, the sky is assumed to be fully overcast (cloud fraction of 1). The cloud optical thickness, cloud phase, effective radius, cloud top height and cloud mask are obtained from the SEVIRI/MSG Cloud Physical Property (CPP) product (Roebeling et al., 2006). This product is available every 15 min. The pixel size of SEVIRI measurement is about 3 km × 6 km (longitude x latitude) in the Netherlands. During one actinic flux profile measurement there are 10 SEVIRI images taken from 11:30 to 13:45 UTC. The cloud properties are selected from every SEVIRI image according to the time and geolocation of the balloon along its trajectory from launching to landing. These ~~time and location~~ times and locations are exactly matching between the SEVIRI images and the radiosonde. Cloud properties ~~at~~ are also selected when the balloon reaches 5 ~~extra points at the start, landing~~special altitudes: surface (launching, landing), cloud top ~~heights (1 in ascendingand 1 in~~ height (ascending, descending), and ~~the highest altitudeof the profile~~ maximum flight altitude. At these 5 points, the cloud properties are selected at the exact geolocation of the balloon but on the ~~nearest measurement time of the SEVIRI images~~ SEVIRI images taken at the time most close to the balloon measurement. The resulting 15 COT values from SEVIRI, ~~sometimes the cloud properties are taken~~ with possibly 2 COT values from one image at two geolocations~~in one image~~, largely follow the COT variations during one profile measurement. The cloud top height is determined from the peak value in the actinic flux profile and is checked with the cloud top height in the SEVIRI data. ~~At small SZA, the peak of the actinic flux profile is very close to~~ Note that the location of the actinic flux peak in cloudy scenes depends primarily on the cloud optical thickness, surface albedo and solar zenith angle (assuming no aerosols). At small solar zenith angle, the actinic flux peak usually occurs slightly below the cloud top for optically thick clouds over dark surface (Madronich, 1987). The cloud base heights are taken from operational ceilometer measurements in De Bilt and Cabauw. The cloud scattering phase matrices were calculated using Mie theory for water droplets and using the effective radius from SEVIRI CPP data. The effective radius and cloud extinction coefficient are assumed to be constant inside the clouds. For example, if the cloud occupies 5 100 m thick layers of the atmospheric model profile and has a COT of 10, then every layer has a COT of 2. The DAK simulations are performed for 15 COT values covering the SEVIRI data. COT of 1 and 100 are also used in the DAK simulations to improve the interpolations.

Although there are 15 collocated COT values from SEVIRI during every actinic flux profile measurement, the COT may not be representative of the actual cloud conditions during an actinic flux profile measurement, because of retrieval uncertainty and subpixel cloud variability. The error of the COT from SEVIRI is about 15 % (http://msgcpp.knmi.nl/mediawiki/index.php/MSGCPP_product_description). Including the mismatching of the SEVIRI measurement and actinic flux profile measurement, the uncertainty of COT estimation during actinic flux profile measurement is probably larger.

In DAK, the altitude levels are specified using the atmospheric profile (height, pressure, temperature) which is taken from the ozone sonde data. In order to get high vertical resolution simulations inside the clouds, the thickness of one atmospheric profile layer is about 100 m for the cloudy atmosphere and coarser ($\sim$ 500 m) for the cloud-free atmosphere. Above 30 km, the atmospheric profile is extended using the mid-latitude summer atmospheric profile (Anderson et al., 1986). The surface albedo is assumed to be 0.15 for grass-covered surface, because the surroundings of the De Bilt site are largely covered by green grass throughout the year. As the altitude of the instrument increases, the surface albedo might change because the instrument sees a larger area. The actinic flux profiles are simulated at different SZA and COT values. Then, the DAK simulated actinic fluxes are interpolated at the actual SZA and COT values along the flight track to get the best simulation for a single measured actinic flux profile.

3.2 Wavelength dependence of actinic flux profile

Because we do not know the exact spectral response of our green LED, we have chosen in this paper the wavelength of 550 nm to represent the wavelength band of the LED. Here a sensitivity study is performed using DAK to check the wavelength dependence of the actinic flux profile. The actinic flux profile is simulated at 450, 500, 550, 600, and 650 nm for a cloudy scene. These wavelengths cover the green LED spectral response completely. The DAK inputs of aerosol, atmospheric profile, ozone and surface albedo data have been described in Sect. 3.1. The water cloud layer is located from 0.8 to 1.3 km altitude and the cloud optical thickness is 30. The particle size (effective radius) of the water clouds is 10 µm. The cloud fraction is 1 (overcast). The extraterrestrial solar irradiance is assumed to be 1 $\mathrm{W m^{-2} nm^{-1}}$ perpendicular to the solar beam for every wavelength in the simulation. The simulated actinic flux profiles for this cloudy case with and without normalization are shown in Fig. 2 at SZA of 30 and 75°, respectively. The normalized actinic flux profiles are the simulated actinic flux profiles divided by the actinic fluxes at 30 km.

As shown in Fig. 2, the simulated actinic fluxes (AF) have a strong wavelength dependence above the cloud due to Rayleigh scattering. Inside the cloud, there is hardly any wavelength dependence of AF because multiple Mie scattering by the cloud particles is dominant. Below the cloud, the wavelength dependence of actinic flux is also small. In this optically thick cloud case, photons scattered above the cloud top cannot easily transmit through the cloud layer; consequently there is almost no wavelength dependence of AF below the cloud. A wavelength dependence of the actinic flux below the cloud only occurs if the cloud is optically thin (say COT of 8).

The actinic flux profiles have similar shape for the 5 wavelengths at SZA = 30° (see Fig. 2a). After normalization at 30 km, the light profiles for different wavelengths almost overlap. Similar behavior occurs at SZA smaller than about 60°. However, when the SZA is getting larger than 60°, the actinic flux profile shape depends strongly on the wavelength. After being normalized at 30 km, the 5 actinic flux profiles have large differences at the cloud top. An example is shown in Fig. 2b for SZA of 75°. This indicates that we can use the actinic flux profile shape at 550 nm to represent the actinic flux profile shape of the wavelength range 450–650 nm at small SZA but not for large SZA.

4 Results

4.1 Actinic flux profile measurements

Actinic flux profiles were measured during 63 launches, of which 30 launches were made in 2006, 27 in 2007, 4 in 2008, and 2 in 2010. The flight trajectories were mainly between 4–9° E and 51–53° N. Most launches had one ascending profile and one descending profile; some launches had only ascending profiles while the descending profiles were not received properly. In the data set there are 14 clear-sky profiles distributed over 9 days and the rest are cloudy profiles.

All the profiles are illustrated in Fig. ~~1a~~3a. The profiles are separated into two groups, because of a calibration issue which occurred in the year 2007. Figure ~~1b~~ 3b shows the ratio between the global irradiance measured at the ground by a pyranometer and the actinic flux at 4 m height (the lowest point of the profile) at 11:30 UTC as a function of SZA. The data points shown as filled circle are measured from 1 June to 21 December 2006. As shown in Fig. ~~1b~~3b, the ratio seems quite consistent in 2006 except for two outliers which are caused by very small actinic fluxes. The scatter of the points in 2006 could be due to partly cloudy scenes. This indicates that the instruments are comparable to each other and the sensors do not depend on the SZA and temperature. The calibration issue can be identified from the ratio in 2007 which appears to ~~be too variablein 2007. The irradiance vs. actinic flux ratio~~ have a different magnitude from that in 2006 and is too variable. The ratio of irradiance to actinic flux at the surface could be used to rule out large instrument errors before launch, ~~however, the~~ such as the calibration issue in 2007. The ratio is not suitable for the calibration of the light sensor ~~. Therefore, in the~~ because the relationship between irradiance and actinic flux is general non-linear (Madronich, 1987). The ratio is dependent on solar zenith angle, surface albedo, and presence of the direct solar beam, which requires cloud and aerosol information. In the comparison with DAK simulated profiles, the measured actinic flux profiles were normalized at 30 km and ~~in~~ are thus in an arbitrary unit.

As shown in Fig. ~~1a~~3a, the actinic flux profiles have large vertical variability below 10 km because of the presence of clouds and aerosols. Above 10 km, the profiles are less variable. The ascending and descending profiles often overlap between 15 and 35 km altitude, because the sonde falls down rapidly after the burst of the balloon. The descending profiles often do not extend down to the surface, because of loss of radio signal at long distance.

4.2 Impact of aerosols and clouds on actinic flux profiles

Figure ~~2a~~ 4a shows four clear-sky actinic flux profiles measured on 11, 12 and 13 September 2006 and 17 April 2010. ~~Figure 2b~~ The clear-sky scenes are determined from MODIS images and Total Sky Imager data at Cabauw. Figure 4b shows the AOT measured at Cabauw for the same days. The smallest SZA values during the actinic flux profile measurements are about 42° on 17 April 2010 and 48° for the measurements in September 2006. According to the lidar extinction coefficient profiles at Cabauw, the boundary layer heights at 11:30 UTC for the 4 days are 1.0 km (17 April 2010), 1.2, 0.5 km, and 0.7 km (11–13 September 2006), respectively. Because the AOT varies during the day (Fig. ~~2b~~4b) we can expect that the AOT also varies along the flight track. On 17 April 2010 the AOT is about 0.1, which is the lowest value in the four days. On this day the actinic flux profile above the boundary layer is also lower than on the other days. The AOT is about 0.3 on 12 September (12:00 UTC) and about 0.4 on 11 and 13 September. This agrees with the actinic flux measurements, namely, the actinic fluxes at 1–5 km on 11 and 13 September are slightly larger than those on 12 September. Due to the scattering by aerosols, the actinic flux is enhanced at the top of the aerosol layer and above. This further demonstrates the consistency of the instruments when the inter-comparison works well. The upper part of the actinic flux profiles (>5 km) has no correlation with the AOT at Cabauw, because of the spatial variation of AOT and surface albedo.

The actinic flux profiles (ascending profiles only) for 6 cloudy cases are shown in Fig. ~~3.~~ 5. The actinic flux profile peaks at the upper boundary of the high relative humidity (RH) layer. Inside clouds, RH values are close to 100 %. RH values at temperatures below 0 °C are corrected to RH with respect to ice, which is larger than the measured RH with respect to water. When the balloon ~~crosses~~ is close to the cloud top, the light sensor detects a sharp peak in the actinic flux profile ~~because of the enhanced light intensity due to multiple scattering~~

~~at the cloud top.~~(e.g. Fig. 5a–d). Inside the cloud, the actinic flux profile decreases until the base of the cloud, and becomes relatively stable below the cloud.

The altitude dependence of the ~~internal radiation field in~~ directional radiation inside a scattering atmosphere or cloud layer depends mainly on the optical depth τ (~~$\tau = 0$ at TOA and $\tau =$ the total atmospheric optical thickness at the surface)and on~~ and its vertical distribution), solar zenith angle and surface albedo (Stammes et al., 1989). The fact that the peak in the ~~actinic~~ diffuse radiative flux is not located at the top of the ~~atmosphere~~ cloud layer but inside the ~~atmosphere~~layer, is due to ~~multiple scattering. Since~~ enhanced multiple scattering in the top layer of clouds. Since direct sunlight is incident at the top of the clouds, the amount of scattered sunlight first increases going from the top downwards due to multiple scattering, reaches a maximum, and then decreases again. In first order, the diffuse radiative flux is linear in τ at the top of the ~~atmosphere~~clouds. It has been found by Stammes et al. (1989) that for an isotropically scattering ~~atmosphere~~ cloud the downward flux increases descending into the ~~atmosphere~~ cloud layer for high sun (~~$\mu_0 > 0.5$~~$\mu_0 > 0.5$), but decreases from the cloud top for low sun (~~$\mu_0 < 0.5$).~~ $\mu_0 < 0.5$). Simulations for actinic fluxes have been done by Madronich (1987) using a simple isotropic model and a Delta-Eddington model. This finding was corroborated with multiple scattering calculations. In the field of actinic flux studies, the peak below the cloud top has been found in actinic flux calculations and in balloon measurements (Van Weele et al., 1995; Van Weele, 1996; Vilà-Guerau de Arellano et al., 1994). ~~Also the solar zenith angle dependence has been found by these authors: in case of a high sun, solar radiation is “trapped” into the atmosphere and photons cannot escape as fast as they enter the cloud. In case of low sun (zenith angles of 52and larger)~~

As can be seen in Figs. 4–5, the actinic flux profiles have small high frequency variations. The variations are relatively larger in cloud-free scenes and above clouds where the instrument is exposed to direct sunlight and smaller inside and below clouds, where mainly diffuse radiation is present. It is probably caused by the rotation of the balloon and the ~~peak in the actinic flux was found to coincide with the cloud top. This known behavior of multiply scattered radiation inside the atmosphere is important to keep in mind when considering~~

~~the AF profilesshown in this paper.~~ light sensor (sphere). The instrument has been adjusted before launch to have less than 2% variation during rotation (see Sect. 2). Therefore, it is interesting to check the relative variation using real profile measurements. The relative variation is determined using the actinic fluxes between 15 and 30 km in every ascending profile. In 63 ascending profiles, 59 profiles have relative variations smaller than 2%; 2 profiles have relative variations of 2.1% and 3.2 %, respectively; 2 profiles were excluded because of not reaching high altitude. The mean variation is 0.7 % for the 61 profiles. If the data between 20 and 25 km are used for the test, the mean variation is also about 0.7 %. This demonstrates that the instrument has a quite uniform response to sunlight.

4.3 Actinic flux profiles compared with surface radiation measurements

Figure ~~4a~~ 6a shows the ratio between the actinic flux below the cloud base close to the surface and at the cloud top (the peak of the actinic flux profile) ~~and below the cloud base close to the surface (~~$\cancel{R_{\mathrm{top/base}}}$($R_{\mathrm{base/top}}$) as a function of the surface solar irradiance measured in De Bilt for 63 ascending profiles. Although some profiles have a calibration issue, this has no impact on ratios calculated from one profile. The ratio $\cancel{R_{\mathrm{top/base}}}$ $R_{\mathrm{base/top}}$ is determined by cloud optical thickness, surface albedo and solar zenith angle.

Similar to the cloud modification factor (CMF) used in UV radiation studies (e.g. Antón et al., 2012), ratios of the actinic flux profiles in cloudy scenes and clear-sky scenes are calculated at cloud top ($\mathrm{CMF_{top}}$) and below the cloud base (close to the ground surface; $\mathrm{CMF_{base}}$). For clear-sky scenes, the CMF is 1 by definition. In principle, the clear-sky actinic flux profile should be calculated using a radiative transfer model using an atmospheric state which is identical to the cloudy scene. Here we used the atmospheric state (temperature, pressure, aerosol optical thickness) on the clear-sky day of 11 September 2006 as a reference for all the cloudy actinic flux profiles in 2006. However, the clear-sky profiles are simulated at the same SZA as occurred for the cloudy profiles. The AOT is not available for cloudy scenes. The AOT is 0.34 on 11 September. According to the scaling factor derived from the clear-sky actinic flux profiles for 11 September 2006, the DAK simulated clear-sky profiles are converted to the same scale as the measured profiles. Otherwise, the calculated CMF would not fulfill the definition of 1 for clear-sky scenes. The simulation of the clear-sky profile is discussed in Sect. 4.4.

In Fig. ~~4b~~ 6b the CMF as a function of COT is shown for cloud top and cloud base, which we denote by CMF_{top} and CMF_{base}. The lines are simulations of CMF_{top} and CMF_{base} for $\text{SZA} = 60^\circ$ and 30° assuming single-layer water clouds (effective droplet radius 8 µm) with cloud top at 2.3 km and cloud base at about 1.5 km. As shown in Fig. ~~4b~~6b, most of the CMFs derived from the measurements are within the ranges of the simulated values. The CMF at cloud base decreases from 1 to about 0.05 with increasing COT. For the actinic flux at the surface, clouds have a shielding effect. The surface albedo is relatively small, so there is not much reflection between the cloud base and surface. Therefore, the optically thicker the clouds, the less light can penetrate the clouds. At COT close to 0, at cloud base there are some CMF_{base} values of 1.4–1.5. This indicates that the actinic fluxes in cloudy scenes are larger than for the clear-sky scenes. This could happen when broken clouds are present and 3-D effects become important. Enhancement of surface actinic flux in the presence of broken clouds has been measured and explained in earlier studies (e.g. Lantz et al., 1996; Crawford et al., 2003). This enhancement can happen if the sun is not obscured by clouds and the diffuse actinic flux of clouds is larger than the diffuse actinic flux of clear-sky (Crawford et al., 2003).

CMF_{top} increases with increasing COT. The enhancement of the actinic flux at cloud top is caused by multiple scattering at cloud top. As illustrated by the simulated CMFs in Fig. 6b, the CMF at cloud top has a stronger SZA dependence than the CMF at cloud base. For example, at COT of 40, from SZA of 30 to 60 °, the CMF changes 0.7 at cloud top and 0.2 at cloud base. This may partly explain the scatter of CMF_{top}. CMF_{top} depends also on the cloud top height due to the height dependence of the clear-sky actinic fluxes. For the measured actinic flux profiles, the cloud top heights are in the range of 1–10 km. At $\text{SZA} = 60^\circ$, the clear-sky actinic fluxes can increase by 10 % from 1 to 10 km and, consequently, the CMF_{top} can change by 10 %. The ~~COT derived from SEVIRI often has a negative bias for partly cloudy scenes, especially for small-scale broken clouds. The~~ outliers of the CMF_{top} at COT < 5 could ~~therefore~~ be due to the ~~COT bias (see Fig. 4b).~~ used COT values. For small local clouds, the COT from SEVIRI may not be presentative for the clouds 'seen' by the light sensor. This can happen because of mismatching between the SEVIRI pixel and balloon location or due to the subpixel clouds in the SEVIRI retrievals.

If the assumed atmospheric state, especially AOT, is not the same as the actual atmospheric state, the CMF may not be 1 at COT $= 0$. According to our simulations, the ratio of clear-sky actinic flux for AOT of 0.25 and of 0.34 is 1.04 at the surface, 0.98 at 1 km, and 0.99 at 10 km for SZA $= 60^\circ$. We estimate that the uncertainty in the CMF due to the AOT uncertainty is up to 5 %.

4.4 Simulations of actinic flux profile for clear-sky scenes

As shown in Fig. ~~2b~~4b, the AOT on 11 September 2006 varies from 0.3 to 0.5 between 11:00 and 14:00 UTC. This may indicate that the AOT is also spatially variable. This is confirmed by MODIS AOT image which reveals a typical spatial variation in AOT between 0.2 and 0.4 for the Netherlands (see Fig. ~~5a~~7a and b). The missing AOT data are mostly caused by presence of clouds. We used the DAK model to simulate actinic flux profiles using AOT values varying from 0 to 0.5. Then the simulated actinic flux profiles are interpolated to the measured AOT and SZA values on 11 September 2006. The simulated and measured actinic flux profiles are shown in Fig. ~~5c~~7c. The simulated actinic flux profile and the measured profile are normalized at 30 km with a scaling factor of 4.13 and 1.002, respectively. The simulated actinic flux profile closely follows the shape of the measured profile, although there are some small deviations. The simulated profile consists of several profiles having different AOT because the balloon moved both vertically and horizontally. In the simulated profile, when the balloon was below 1 km, the AOT was 0.5, after the balloon moved above 1 km, the AOT is 0.34. AOT values of 0.5 and 0.34 occur at different locations, not in one vertical profile. As shown in the trajectory in Fig. ~~5b~~7b, the measured actinic flux profile is in fact three-dimensional, because the sonde drifts away from the launch location. This feature is more significant during cloudy conditions due to the large spatial variation of cloud optical thickness.

4.5 Simulations of actinic flux profiles for fully cloudy scenes

Global irradiances derived from SEVIRI, called surface solar irradiances (SSI), are calculated using the SEVIRI COT derived from the CPP algorithm and aerosols from a monthly climatology (Greuell et al., 2013). In order to check the quality of the SEVIRI COT in the SSI calculations, we compared the SEVIRI SSI with the ground-based shortwave global irradiance measurement at De Bilt. On the 63 actinic flux profile measurement days, we compared SEVIRI SSI at 11:30 UTC with ground-based 10 min mean (11:30–11:40 UTC) pyranometer measurements of global irradiance in De Bilt. As shown in Fig. ~~6~~8, the SEVIRI SSI and ground-based measurements agree well with a correlation coefficient of 0.965 and a bias of 22 $\mathrm{W\,m^{-2}}$ (for the mean SSI). This suggests that the COT from SEVIRI is of good quality and the actinic flux profiles calculated using these COTs can be realistic. The mean SSI value of 4 SEVIRI pixels and the nearest single pixel SSI are often quite different for SSI values between 200 and 800 $\mathrm{W\,m^{-2}}$. This is caused by the inhomogeneity of clouds. The cases where SSI $< 200\,\mathrm{W\,m^{-2}}$ or SSI $> 800\,\mathrm{W\,m^{-2}}$ usually correspond to fully cloudy or clear-sky scenes, respectively. Therefore, the COT of the single SEVIRI pixel that is most close to the balloon measurement time and location may not be representative of the clouds that actually determine the actinic flux profile.

The cloudy actinic flux profiles are simulated for 5 single-layer water cloud cases in 2006, of which the results are shown in Figs. ~~7–11~~9–13. The original actinic flux profiles (without normalization) have already been shown in Fig. ~~3.~~ 5. The simulations are presented in the order of complexity of the cases. We start with the simplest case on 5 September (Fig. ~~7~~9), which is followed by an optically very thick cloudy case on 15 June (Fig. ~~8~~10). During these launches, the COT mainly decreased during the balloon flight. On 22 June (Fig. ~~9~~11) and 10 August (Fig. ~~10~~12), the COT increased after launch and decreased when the balloon was at its maximum height. On 22 December (Fig. ~~11~~13) the cloud layer was low and stable but the SZA was large ($> 75^{\circ}$).

On 5 September 2006, the prevailing winds were from the west, so the balloon drifted eastwards. The SEVIRI cloud optical thickness images of 11:30 UTC and 13:00 UTC are the closest to the start and end of the ascending profile. As shown in Fig. ~~7a~~ 9a it was fully cloudy in De Bilt at 11:30 UTC when the ozone sonde was launched. The cloud optical thickness at 11:30 UTC was about 25. The clouds were optically thicker in the north-east and optically thinner south of De Bilt. At 13:00 UTC the balloon drifted towards an area with COT of about 10 (see Fig. ~~7b~~9b). In the first 30 min, the balloon flew over clouds having similar COT, then the clouds became thinner.

The COT for the trajectory of the balloon is shown as a function of balloon altitude in Fig. ~~7c~~9c. The SEVIRI pixels are selected within 0.1° of the balloon lat/lon box which usually has up to 5 pixels. The number of SEVIRI pixels can be less than 5 because of missing COT data (clear-sky scene or no retrieval). Please note that the COT values in the maps are averaged over $0.1^\circ \times 0.1^\circ$ grids, while the COT values in Fig. ~~7c~~ 9c are given for ~~single pixels~~every SEVIRI pixel.

If the balloon is above the cloud layer, variations in cloud optical thickness and cloud height will not produce sharp peaks in the actinic flux profile. However, all cloud variations along the flight track will show up in the actinic flux profile, because it includes the radiation from all directions and heights. The measured actinic flux profile in Fig. ~~7d~~ 9d shows two peaks, one at about 0.5 km, another at about 2 km. This indicates that there are two cloud layers, with cloud top heights at about 0.5 and 2 km, respectively. This is confirmed by the radar measurements at Cabauw, which show one cloud layer at 0.3–0.5 km and another cloud layer at 1–2 km.

In the simulations the clouds are assumed to be single-layer, with cloud top height at 2 km and cloud base height at 1 km. Therefore, the simulated actinic flux profile has a single peak at 2 km. The COT values used in the simulations are shown in Fig. ~~7c~~ 9c by the black line. The simulated actinic flux profile is in good agreement with the measured flux profile. Although the measured and simulated actinic flux profiles are both normalized at 30 km, this does not influence the shapes of the profiles. The consistency between the SEVIRI SSI and the ground-based global irradiance measurements suggest that the COT at De Bilt is quite representative. During the flight, the SZA changes from 29° to 34°, which has been taken into account in the simulation. The variation in the actinic flux profile shape is mainly due to variation in the COT.

The COT values and the measured and simulated actinic flux profiles for 15 June 2006 are shown in Fig. ~~8.~~ 10. The mean COT was very high, 95, at the launch in De Bilt and the actinic flux profile shows a very strong peak at 1.5 km. The balloon drifted to the north, then turned west, and reached an altitude of about 30 km over a region where the COT is small. The dips in the actinic flux profile at 2 and 4 km are probably related to optically thin clouds, cloud holes, cloud shadows or clear-sky regions (Los et al., 1997).

The cloud top and base heights in simulation were at 1.5 and 0.5 km, respectively. The dips at 2 and 4 km were ignored in the simulation. As shown by the SEVIRI images of COT (Figs. ~~8a~~ 10a and b), clouds were getting thinner during the flight. The change of the measured actinic flux profile at 10 km suggests the change of COT but unfortunately there is no SEVIRI image available at this time. Therefore, the COT is extrapolated at this altitude. Above 10 km, the SEVIRI COT had to be reduced from about 30 to 20 to get a better simulation. Since the COT used in the simulation allows for closure with the measured ground-based global irradiance, the COT values used for the actinic flux profile simulation are possibly correct. In view of the uncertainty in the SEVIRI COT retrieval, the mentioned adjustment is also reasonable.

On 22 June 2006, the spatial variability in the SEVIRI COT along the balloon flight track is considerable (Figs. ~~9a~~ 11a and b). As shown in Fig. ~~9c~~11c, the COT decreases along the flight track and shows a large scatter. Between 10 and 20 km altitude, there are often only 2 COT values available in the ~~1-degree~~ 0.1-degree box in the SEVIRI image instead of 4 COT values, which suggests some clear-sky pixels. At launch the COT is about 30 and at 2 km altitude the COT decreases slightly. ~~The simulated~~ In the simulation, the cloud top height and base height are 3 and 2 km, respectively. When the balloon passed through the cloud top, the flux profile showed a sharp peak at 3 km. ~~The COT increased again at about~~ When the balloon was flying at 4 km, ~~forming a broad peak~~ the COT of underlying clouds increased, forming the broad peak at 3–6 km in the actinic flux profile~~at 3–6~~. The simulated actinic flux profile follows the measured actinic flux profile shape very well. The actinic flux profile below cloud top decreases in two steps, which does not occur in the simulated profile~~because the extinction coefficient is assumed to be constant within the cloud~~ . According to the measured actinic flux profile, cloud base could be at 1 km and the cloud optical thickness increases during the ascent from 1–3 km.

On 10 August 2006 (Fig. ~~10~~12), the clouds are optically thinner than the clouds described in the previous cases. According to SEVIRI, the COT is only about 15 at the launch in De Bilt. The main cloud layer is at 3 km. As can be seen from Fig. ~~10d~~12d, the balloon went through several cloud layers between 2 and 5 km. The balloon passed over some optically thin clouds when it was at 5–10 km altitude, then the COT increased again. The simulated cloud base and top heights are 2 and 3 km, respectively. As shown in Fig. ~~10d the largest peak of the measured~~ 12d the simulated actinic flux profile ~~and~~ follows the general shape of the ~~profile are properly simulated~~measured profile and the largest peak in the measurement is being reproduced in the simulation.

The previously described cases all have SZA smaller than 60°, so the application of a pseudo-spherical correction is not needed. However, during the actinic flux profile measurement on 21 December 2006 (Fig. ~~11~~13), the SZA values ranged between 75° and 78°, therefore the pseudo-spherical correction has to be applied in the actinic flux profile simulations. Based on radar measurements in Cabauw, the cloud layer was very close to the ground surface and the cloud top height was 1 km. Although it was winter, the surface temperature was about 7 °C at the launch in De Bilt and there was no snow on the surface. As presented in Fig. ~~11a~~ 13a the SEVIRI COT is about 30 in De Bilt and relatively stable until the balloon reaches an altitude of 20 km, where the COT starts to decrease. The pixel-to-pixel variation of COT is small. Therefore, this should be a simple case to simulate. As shown in Fig. ~~11d~~13d, the simulated actinic profile agrees well with the measured profile shape above 10 km and below the cloud top. However, the simulated actinic flux profile from cloud top (1.5 km) to about 10 km is much smaller than the measured actinic flux profile. ~~Apparently, some light is missing in the DAK simulations. Usually, the simulated actinic flux above clouds increases with increasing COT, but in~~ As discussed in Sect. 3, for this case the ~~actinic flux does not increase that much at SZA $>$ 75, even if the COT is increased~~

~~up to 100. It is conceivable that the full spherical geometry of the atmosphere has to be taken into account.~~ wavelength dependence of actinic flux is important. The agreement between simulated and observed actinic flux profile might be improved if the simulations were performed at a fine wavelength grid and convolved with the spectral response function of the LED. The simulations should also use the solar irradiance spectrum over the LED spectral range instead of a constant value (1 $\mathrm{W m^{-2} nm^{-1}}$) used in this paper.

~~Another~~ A challenge for the DAK model appears to be the simulation of the actinic flux profile of 6 September 2006 (see Fig. ~~3e~~5e). The actinic flux profile of this day is similar to the clear-sky profiles, without sharp peaks. However, the value of the actinic flux profile above cloud top is larger than for the clear-sky scenes. According to the total sky imager data at Cabauw and MODIS Terra 1 km resolution imagery, there were many small broken clouds on this day. Since SEVIRI cannot resolve the small broken clouds, the COT is quite low, about 1–3. This case probably requires a 3-D radiative transfer model for correctly simulating the actinic flux profile.

The simulated actinic flux ratio (cloudy/clear-sky) (CMF) for the cloudy cases of Figs. 9–13 are presented in Fig. 14. The simulated cloudy actinic flux profiles have already been shown in Figs. 9–13 after normalization. The variation of CMF in a single profile is mainly caused by the cloud optical thickness. The differences of the CMFs in the 5 cases include the impact of SZA, COT, cloud vertical distribution and cloud scattering phase matrices, because the other DAK input data are the same for these cases. As shown in Fig. 14, the CMFs are larger than 1 above the cloud top and smaller than 1 below the cloud base. The maximum CMF happens just below the cloud top and decreases almost linearly towards the cloud base. Following Madronich (1987) the features in Fig. 14 can be well understood. The actinic flux above clouds is larger than the clear-sky value because the effective albedo of cloud and surface together is greater than the surface albedo alone. Since the low cloud layers in Figs. 9–13 are all optically thick clouds, the incident light at cloud top cannot easily transmit through the cloud layer. Therefore, the CMFs are smaller than 1 below cloud base. Inside clouds, the peak of CMF happens in a layer below cloud top where the direct incident light is strongly reduced but has given rise to a diffuse downward flux while the lower part of the cloud is still optically thick. In this case the lower part of the clouds creates a high albedo, the top layer of the cloud reflects downward the reflected light again. These components of the diffuse radiation field create a strong enhancement inside the cloud.

5 Conclusions

A green light sensor has been developed and launched from De Bilt on an ozone sonde balloon between June 2006 and April 2010. Several copies of this sensor were calibrated to one reference sensor to make them intercomparable, although not absolutely calibrated. The calibration failed in 2007, therefore mainly the 2006 data (ascending profiles) were used in the analysis. The instrument is not sensitive to ozone and water vapor and it is temperature-stabilized. In total there were 63 launches (one ascending profile and one descending profile per launch), of which 9 launches were made during clear-sky conditions. The other launches were made through cloudy atmospheres. The actinic flux profiles contain very little noise and the impact of clouds on the actinic flux profile could be clearly detected.

The actinic flux profile reveals an large enhancement at the cloud top. Above the cloud top, the actinic flux profile is still influenced by the clouds but the enhancement is smaller than at the cloud top. The actinic flux profile decreases from the cloud top to cloud base, almost linearly. Below the cloud base, the actinic flux profile is relatively constant, especially for the low clouds. The balloon often passed through several layers of clouds. Therefore, the actinic flux of different heights reflects different cloud conditions along the flight track. The impact of cloud is quantified by the cloud modification factor (CMF). The CMF is in the range of 1–2.3 at the cloud top and 1–0.1 at the cloud base. The CMF depends on cloud properties and SZA. The measured CMF values agree with the DAK simulated CMF, especially for cloud base CMF. The CMF at the cloud top is more complicated because sometimes the location of the cloud top can be ambiguous due to the horizontal movement of the balloon in the clouds or due to holes in vertical direction (broken clouds). For the calculation of the clear-sky actinic flux, the same aerosol setting has been used for all cloudy cases, which could cause a small (5 %) uncertainty in the CMF.

The actinic flux profiles for single-layer water clouds during fully cloudy conditions were simulated using DAK. The shapes of simulated actinic flux profiles are in good agreement with the actinic flux profile measurements, except for SZA $> 75^\circ$. The most important input for the simulation is the COT along the flight track, which was obtained from 15 min SEVIRI observations. However, when the optical properties of the clouds are variable at the pixel-to-pixel scale, the SEVIRI COT has to be modified to get a better simulation of the actinic flux profile. Because of the good agreement between the measured and simulated actinic flux profile shapes, it would be possible to convert the measured actinic flux profile to absolute values.

For clear-sky conditions, the most important factors determining the shape and magnitude of the actinic flux profiles are SZA, surface albedo, aerosol optical thickness and aerosol height. Using the aerosol optical thickness data for Cabauw, the measured actinic flux profiles could be simulated reasonably well. The simulations could be improved if we would have aerosol data along the flight track of the balloon.

The green light sensor that we used for the actinic flux profile measurements is cheap and stable. In combination with a ground-based irradiance measurement and retrieved COT from SEVIRI, actinic flux profiles can be calculated. The light sensor is useful for the evaluation of the impact of clouds on actinic flux profiles. Applications of measured actinic flux profiles and simultaneous ozone and NO_2 profiles (Sluis et al., 2010) in atmospheric chemistry models will be studied in the future.

Acknowledgements. We would like to thank our colleague M. van Weele (KNMI) for his comments and suggestions about the manuscript. We appreciate J. F. Meirink (KNMI) for his help with the SEVIRI CPP product, available on http://msgcpp.knmi.nl. We acknowledge the MODIS mission scientists and associated NASA personnel for the production of the MODIS AOT data. This research is supported by NWO (Netherlands Organization for Scientific Research) through the GO project “Cloud radiative forcing profile and vertical energy redistribution in the atmosphere (CRAFT)”, project number ALW-GO-AO/09-22.

References

Anderson, G. P., Clough, S. A., Kneizys, F. X., Chetwynd, J. H., and Shettle, E. P.: AFGL atmospheric constituent profiles, Tech. Rep. AFGL-TR-86-0110, Air Force Geophys. Lab., Hanscom AFB, Mass, 1986.

Antón, M., Alados-Arboledas, L., Guerrero-Rascado, J. L., Costa, M. J., C Chiu, J., and Olmo, F. J.: Experimental and modeled UV erythemal irradiance under overcast conditions: the role of cloud optical depth, Atmos. Chem. Phys., 12, 11723–11732, doi:10.5194/acp-12-11723-2012, 2012.

Bodhaine, B.A., Wood, N.B., Dutton, E.G., and Slusser, J.R.: On Rayleigh optical depth calculations, J. Atmos. Oceanic Technol., 16, 1854–1861, doi: http://dx.doi.org/10.1175/1520-0426(1999)016<1854:ORODC>2.0.CO;2, 1999.

Brooks, D. R. and Mims III, F. M.: Development of an inexpensive handheld LED-based Sun photometer for the GLOBE program, J. Geophys. Res., 106(D5), 4733–4740, doi:10.1029/2000JD900545, 2001.

Calbó, J., Pagès, D., and González, J.-A.: Empirical studies of cloud effects on UV radiation: a review, Rev. Geophys., 43, RG2002, doi:10.1029/2004RG000155, 2005.

Cantrell, C. A., Shetter, R. E., Calvert, J. G., Parrish, D. D., Fehsenfeld, F. C., Goldan, P. D., Kuster, W., Williams, E. J., Westberg, H. H., Allwine, G., Martin, R.: Peroxy radicals as measured in ROSE and estimated from photostationary state deviations, J. Geophys. Res., 98, 18355–18366, doi:10.1029/93JD01794, 1993.

Crawford, J., Shetter, R. E., Lefer, B., Cantrell, C., Junkermann, W., Madronich, S., and Calvert, J.: Clouds and trace gas distributions during TRACE-P, J. Geophys. Res., 108, 8818, doi:10.1029/2002JD003177, D21, 2003.

Crutzen, P. J. and Zimmermann, P. H.: The changing photochemistry of the troposphere, Tellus B, 43, 136–151, doi:10.1034/j.1600-0889.1991.t01-1-00012.x, 1991.

De Haan, J. F., Bosma, P. B., and Hovenier, J. W.: The adding method for multiple scattering computations of polarized light, Astron. Astrophys., 183, 371–391, 1987.

De Roode, S. R., Duynkerke, P. G., Boot, W., and Van der Hage, J. C. H.: Surface and tethered-balloon observations of actinic flux: effects of arctic stratus, surface albedo, and solar zenith angle, J. Geophys. Res., 106, 27497–27507, doi:10.1029/2001JD900236, 2001.

Eskes, H., van Velthoven, P., Valks, P., and Kelder, H.: Assimilation of GOME total ozone satellite observations in a three-dimensional tracer transport model, Q. J. Roy. Meteor. Soc., 129, 1663–1681, doi:10.1256/qj.02.14, 2003.

Greuell, W., Meirink, J. F., and Wang, P.: Retrieval and validation of global, direct, and diffuse irradiance derived from SEVIRI satellite observations, J. Geophys. Res.-Atmos., 118, 2340–2361, doi:10.1002/jgrd.50194, 2013.

Hofzumahaus, A., Kraus, A. , Kylling, A. and Zerefos, C.: Solar actinic radiation (280–420 nm) in the cloud-free troposphere between ground and 12 km altitude: Measurements and model results, J. Geophys. Res., 107, doi=10.1029/2001JD900142, 2002.

Johnston, H. S., personal communication (1997) to E.-P. Röth, R. Ruhnke, G. Moortgat, R. Meller, and W. Schneider, Berichte des Forschungszentrums Jülich, jül-3340, 1997. (http://satellite.mpic.de/spectral_atlas/cross_sections/Ozone/O3_Johnston(1997)_298K_408-599nm.txt)

Junkermann, W.: Measurements of the J(O^{1}D) actinic flux within and above stratiform clouds and above snow surfaces, Geophys. Res. Lett., 21, 793–796, doi:10.1029/93GL03498, 1994.

Kazadzis, S., Bais, A. F., Balis, D., Zerefos, C. S., and Blumthaler, M.: Retrieval of downwelling UV actinic flux density spectra from spectral measurements of global and direct solar UV irradiance, J. Geophys. Res., 105, 4857–4864, 2000.

Kylling, A., Albold, A., Seckmeyer, G.: Transmittance of a cloud is wavelength-dependent in the UV-range: Physical interpretation, Geophys. Res. Lett., 24, 397–400, DOI: 10.1029/97GL00111, 1997.

Kylling, A., Danielsen, T., Blumthaler, M., Schreder, J., and Johnsen, B.: Twilight tropospheric and stratospheric photodissociation rates derived from balloon borne radiation measurements, Atmos. Chem. Phys., 3, 377-385, doi:10.5194/acp-3-377-2003, 2003.

Kylling, A., Webb, A. R., Kift, R., Gobbi, G. P., Ammannato, L., Barnaba, F., Bais, A., Kazadzis, S., Wendisch, M., Jäkel, E., Schmidt, S., Kniffka, A., Thiel, S., Junkermann, W., Blumthaler, M., Silbernagl, R., Schallhart, B., Schmitt, R., Kjeldstad, B., Thorseth, T. M., Scheirer, R., and Mayer, B.: Spectral actinic flux in the lower troposphere: measurement and 1-D simulations for cloudless, broken cloud and overcast situations, Atmos. Chem. Phys., 5, 1975–1997, doi:10.5194/acp-5-1975-2005, 2005.

Lantz, K. O., Shetter, R. E., Cantrell, C. A., Flocke, S. J., Calvert, J. G. and Madronich, S.: Theoretical, actinometric, and radiometric determinations of the photolysis rate coefficient of NO_2 during the Mauna Loa Observatory Photochemistry Experiment 2, J. Geophys. Res., 101(D9), 14613–14630, doi:10.1029/96JD00215, 1996.

Los, A., van Weele, M., and Duynkerke, P. G.: Actinic fluxes in broken cloud fields, J. Geophys. Res., 102, 4257–4266, doi:10.1029/96JD03123, 1997.

Madronich, S.: Photodissociation in the atmosphere 1. Actinic flux and the effect of ground reflections and clouds, J. Geophys. Res., 92, 9740–9752, doi:10.1029/JD092iD08p09740, 1987.

Mannschreck, K., Gilge, S., Plass-Duelmer, C., Fricke, W., and Berresheim, H.: Assessment of the applicability of NO-NO_2-O_3 photostationary state to long-term measurements at the Hohenpeissenberg GAW Station, Germany, Atmos. Chem. Phys., 4, 1265–1277, doi:10.5194/acp-4-1265-2004, 2004.

Mateos, D., Pace, G., Meloni, D., Bilbao, J., di Sarra, A., de Miguel, A., Casasanta, G., and Min, Q.: Observed influence of liquid cloud microphysical properties on ultraviolet surface radiation, J. Geophys. Res.-Atmos., 119, 2429–2440, doi:10.1002/2013JD020309, 2014.

Mayer, B., Kylling, A., Madronich, S., and Seckmeyer, G.: Enhanced absorption of UV radiation due to multiple scattering in clouds: experimental evidence and theoretical explanation, J. Geophys. Res., 103, 31241–31254, doi:10.1029/98JD02676, 1998.

McKenzie, R. L., Johnston, P. V., Smile, D., Bodhaine, B. A., and Madronich, S.: Altitude effects on UV spectral radiance deduced from measurements at Lauder, New Zealand, and Mauna Loa Observatory, Hawaii, J. Geophys. Res., 106, 22845–22860, doi:10.1029/2001JD900135, 2001.

Palancar, G. G., Shetter, R. E., Hall, S. R., Toselli, B. M., and Madronich, S.: Ultraviolet actinic flux in clear and cloudy atmospheres: model calculations and aircraft-based measurements, Atmos. Chem. Phys., 11, 5457–5469, doi:10.5194/acp-11-5457-2011, 2011.

Roebeling, R. A., Feijt, A. J., and Stammes, P.: Cloud property retrievals for climate monitoring: implications of differences between Spinning Enhanced Visible and Infrared Imager (SEVIRI) on Meteosat-8 and Advanced Very High Resolution Radiometer (AVHRR) on NOAA-17, J. Geophys. Res., 111, D20210, doi:10.1029/2005JD006990, 2006.

Schwander, H., Koepke, P., Kaifel, A., and Seckmeyer, G.: Modification of spectral UV irradiance by clouds, J. Geophys. Res., 107, 4296, doi:10.1029/2001JD001297, 2002.

Schiller, C., Hofzumahaus,A.,Müller, M., Klein, E. , Röth, E.–P., and Schmidt, U.: Ultraviolet actinic flux in the stratosphere: An overview of balloon-borne measurements during EASOE, 1991/92, Geophys. Res. Lett., 21, 1239–1242, 1994.

Seckmeyer, G., Erb, R., and Albold, A.: Transmittance of a cloud is wavelength-dependent in the UV-range, Geophys. Res. Lett., 23, 2753–2755, 1996.

Sluis, W. W., Allaart, M. A. F., Piters, A. J. M., and Gast, L. F. L.: The development of a nitrogen dioxide sonde, Atmos. Meas. Tech., 3, 1753–1762, doi:10.5194/amt-3-1753-2010, 2010.

Stammes, P.: Spectral radiance modelling in the UV-Visible range, in: IRS 2000: Current Problems in Atmospheric Radiation, edited by: Smith, W. L. and Timofeyev, Y. M., A. Deepak Publ., Hampton, VA, 385–388, 2001.

Stammes, P., de Haan, J. F., and Hovenier, J. W.: The polarized internal radiation field of a planetary atmosphere, Astron. Astrophys., 225, 239–259, 1989.

Wang, P., Knap, W. H., Kuipers-Munneke, P., and Stammes, P.: Clear-sky shortwave radiative closure for the Cabauw Baseline Surface Radiation Network site, the Netherlands, J. Geophys. Res., 114, D14206, doi:10.1029/2009JD011978, 2009.

Wang, P., Knap, W. H., and Stammes, P.: Cloudy-sky shortwave radiative closure for a Baseline Surface Radiation Network site, J. Geophys. Res., 116, D08202, doi:10.1029/2010JD015141, 2011.

Van Weele, M.: Effect of clouds on ultraviolet radiation, photodissociation rates of chemical species in the troposphere, Ph.D. thesis, University of Utrecht, Utrecht, the Netherlands, 1996.

Van Weele, M., Vilà-Guerau de Arellano, J., and Kuik, F.: Combined measurements of UV-A actinic flux, UV-A irradiance and global radiation in relation to photodissociation rates, Tellus B, 47, 353–364, doi:10.1034/j.1600-0889.47.issue3.6.x, 1995.

Vilà-Guerau de Arellano, J., Duynkerke, P. G., and van Weele, M.: Tethered-balloon measurements of actinic flux in a cloud-capped marine boundary layer, J. Geophys. Res., 99, 3699–3705, doi:10.1029/93JD03090, 1994.

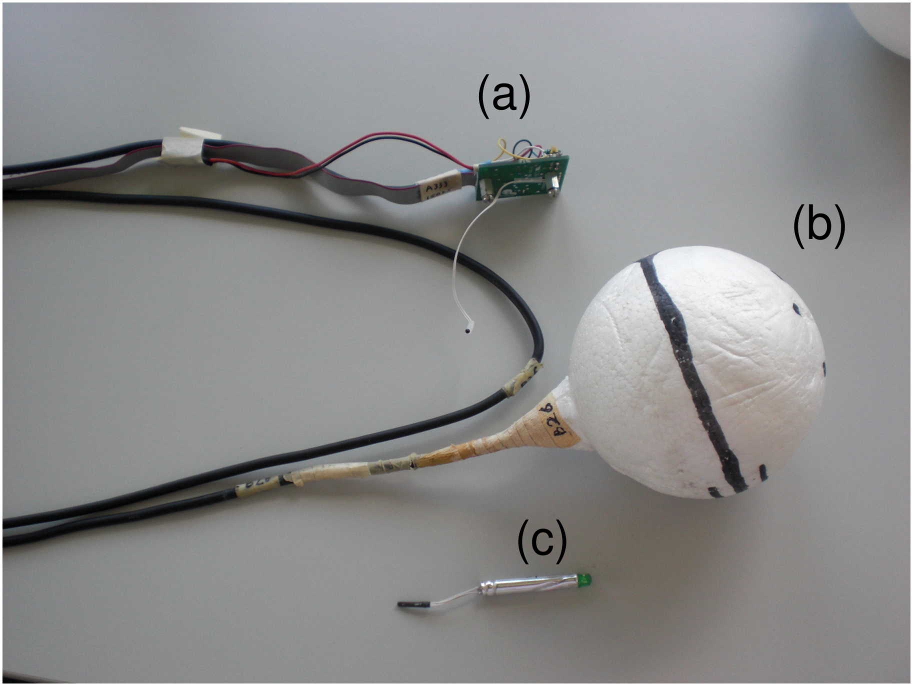

Figure 1. Photo of the light sensor: **(a)** data transmitter, **(b)** sphere, **(c)** green LED.

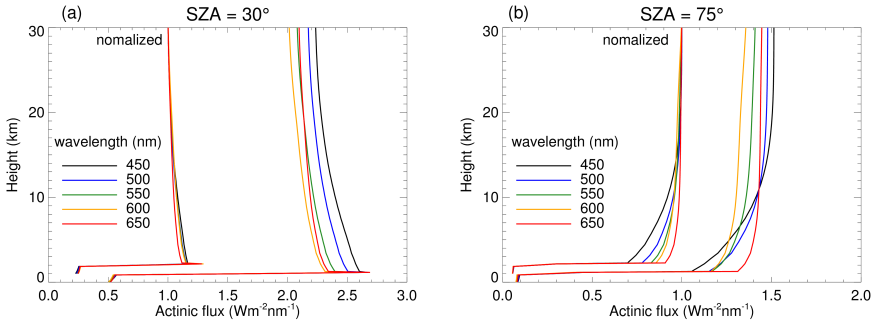

Figure 2. Simulated actinic flux profiles at wavelengths: 450, 500, 550, 600, 650 nm at SZA = **(a)** 30 and **(b)** 75 °. The cloud top is at 1.3 km, cloud base is at 0.8 km, cloud optical thickness is 30. Particle size of the water clouds is 10 µm. The aerosol optical thickness is 0.18 at 550 nm and surface albedo is 0.15. At every wavelength the normalized actinic flux profile is the simulated actinic flux profile divided by the actinic flux at 30 km. The normalized actinic fluxes are shifted 1 km up in the y-axis.

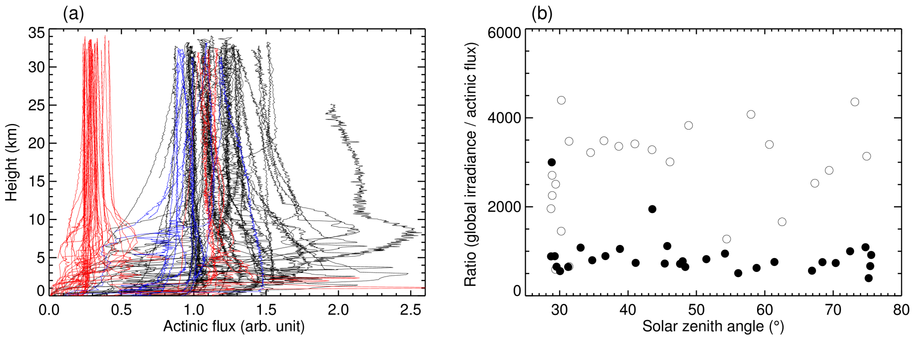

Figure 3. (a) Measured actinic flux profiles in 2006 (black lines), 2007 (red lines), 2008 and 2010 (blue lines). **(b)** Ratio between the global irradiance at the ground measured at 11:30 UTC at De Bilt and the actinic flux profile measurement at 4 m height at 11:30 UTC at De Bilt. Results for 2006 are marked as filled circles, results for 2007 are in open circles.

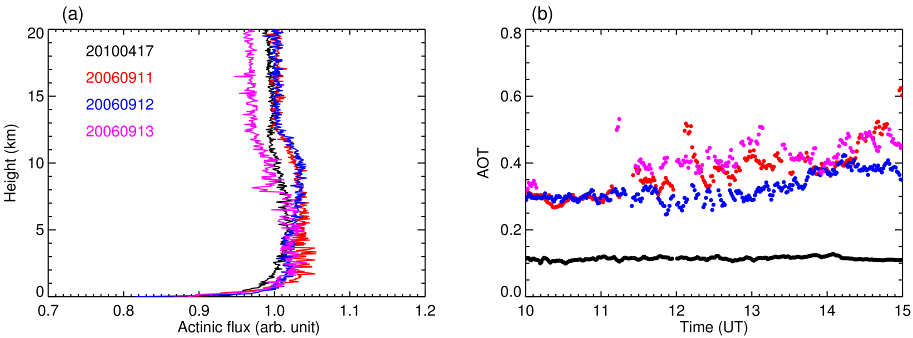

Figure 4. (a) Clear-sky actinic flux profiles measured on 11–13 September 2006 and 17 April 2010. **(b)** AOT at 501 nm measured in Cabauw for the same days. The profiles are the original measurements, not ~~being~~ normalized.

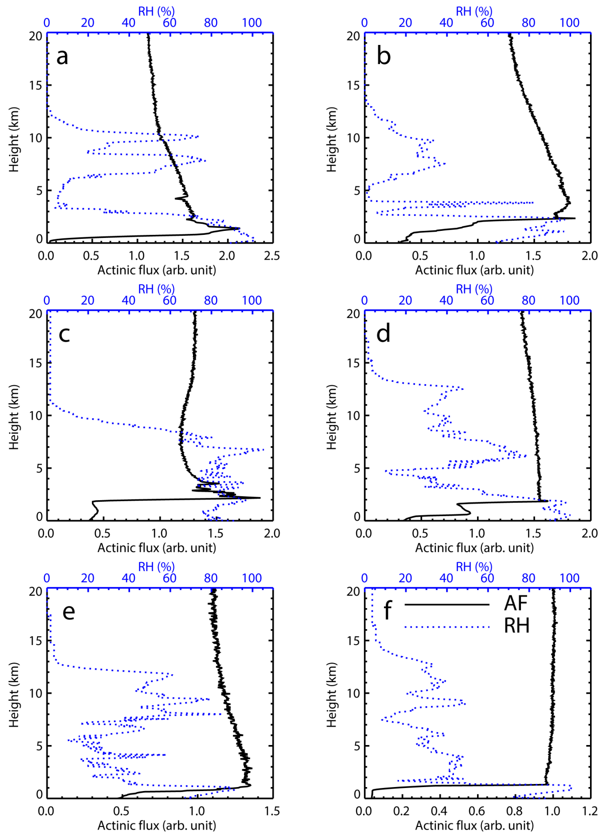

Figure 5. Actinic flux (AF) and relative humidity (RH) profiles for cloudy scenes measured on **(a)** 15 June 2006, SZA $= 28.8°$, **(b)** 22 June 2006, SZA $= 28.7°$, **(c)** 10 August 2006, SZA $= 36.7°$, **(d)** 5 September 2006, SZA $= 45.4°$, **(e)** 6 September 2006, SZA $= 45.7°$, and **(f)** 21 December 2006, SZA $= 75.6°$. The profiles are ascending measurements and are not normalized. The SZA value is at 11:30 UTC, the start of the profile.

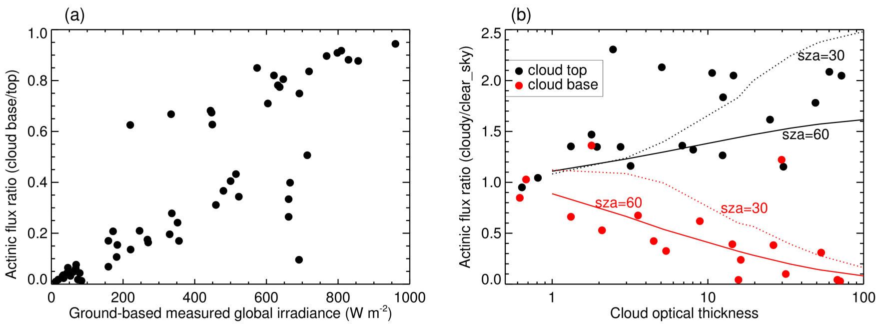

Figure 6. (a) Ratio between the measured actinic fluxes at cloud ~~top~~ base and at cloud ~~base~~ top vs. the measured global irradiance at the surface, for all data. **(b)** Ratio between measured actinic fluxes of cloudy and clear-sky scenes (CMF) at cloud top (black) and cloud base (red) vs. SEVIRI cloud optical thickness at 11:30 UTC for data in 2006. The dots are measurements, the lines are simulations for CMF at cloud top and cloud base for SZA = 30 and 60 °.

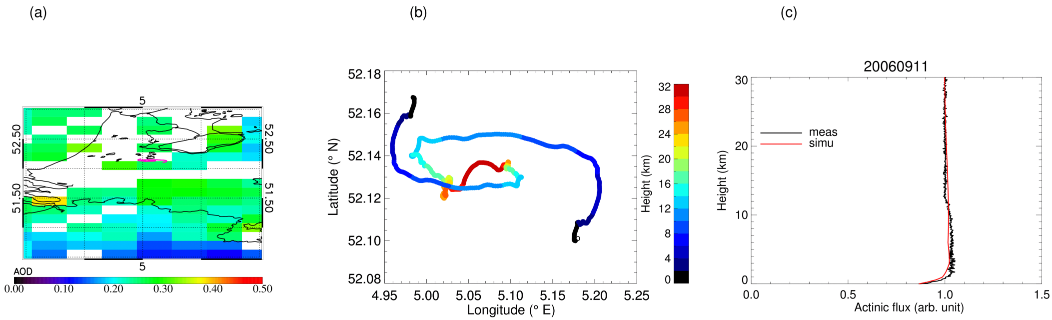

Figure 7. Clear-sky case on 11 September 2006. **(a)** MODIS ~~AOT~~ aerosol optical thickness image at 11:45 UTC, the purple curve shows the trajectory of the balloon. **(b)** Trajectory of the balloon, with its height indicated by color. The location of De Bilt is marked with a circle. **(c)** Measured actinic flux profile and simulated actinic flux profile.

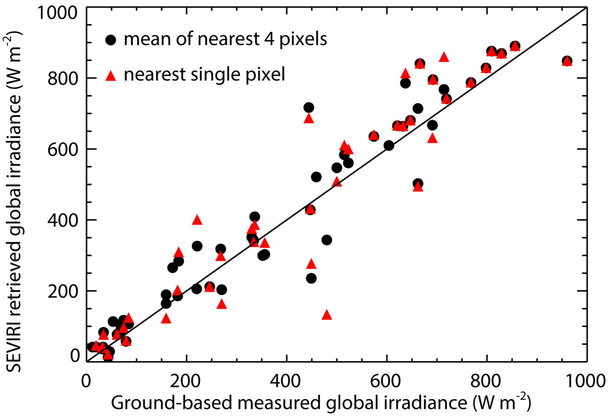

Figure 8. Scatter plot of SEVIRI retrieved global irradiance at the surface (surface solar irradiance, SSI) vs. ground-based measured global irradiance at 11:30 UTC at De Bilt on all 63 actinic flux profile measurement days. The black line is the one-to-one line. The black dots indicate the mean SSI of all SEVIRI pixels in a $0.1^\circ \times 0.1^\circ$ (latitude $\times$ longitude) grid box. The red triangles indicates the nearest single pixel SSI in the grid box.

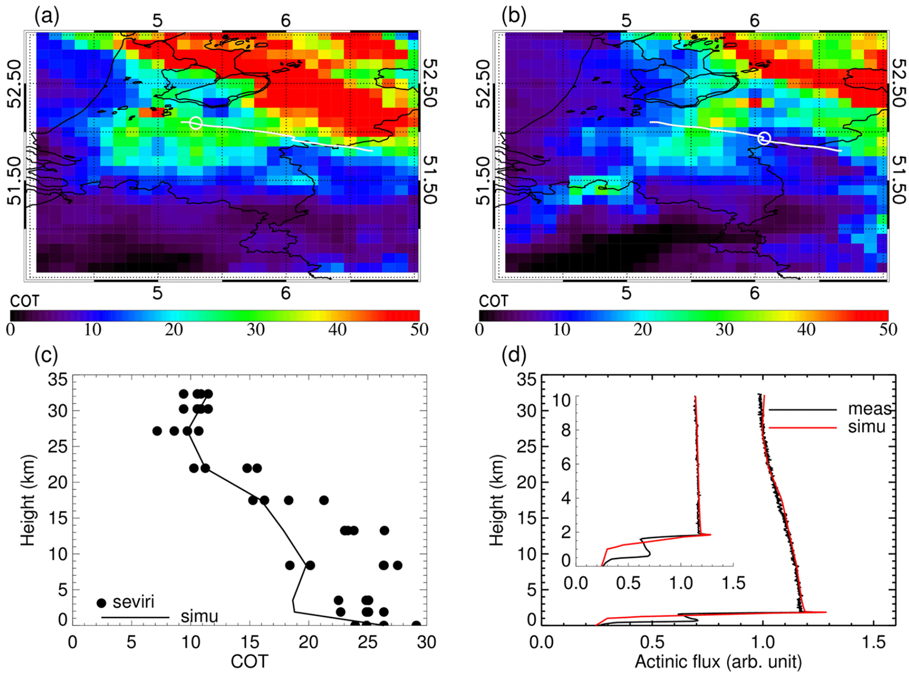

Figure 9. Cloudy sky case on 5 September 2006. **(a)** SEVIRI cloud optical thickness image at 11:30 UTC (balloon launch) and **(b)** at 13:00 UTC (balloon maximum height). The flight track of balloon is indicated as a white line. The location of balloon at the time the SEVIRI image is taken is indicated as a white circle. **(c)** SEVIRI single pixel cloud optical thickness values in $0.1^\circ \times 0.1^\circ$ (latitude $\times$ longitude) boxes along the trajectory of the balloon (dots) as a function of the height of the balloon. The COT values used in the simulations are connected by the black line. **(d)** Measured actinic flux profile and simulated actinic flux profile (both normalized at 30 km altitude, respectively). The actinic flux profile is also shown zoomed-in at 0–10 km.

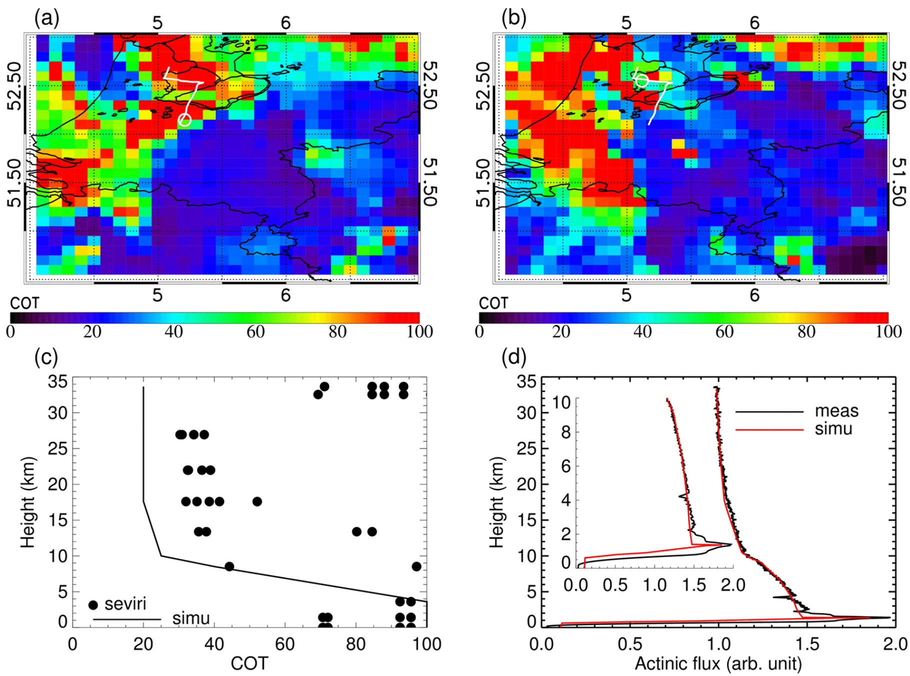

Figure 10. Same as Fig. ~~7~~ 9 but for 15 June 2006.

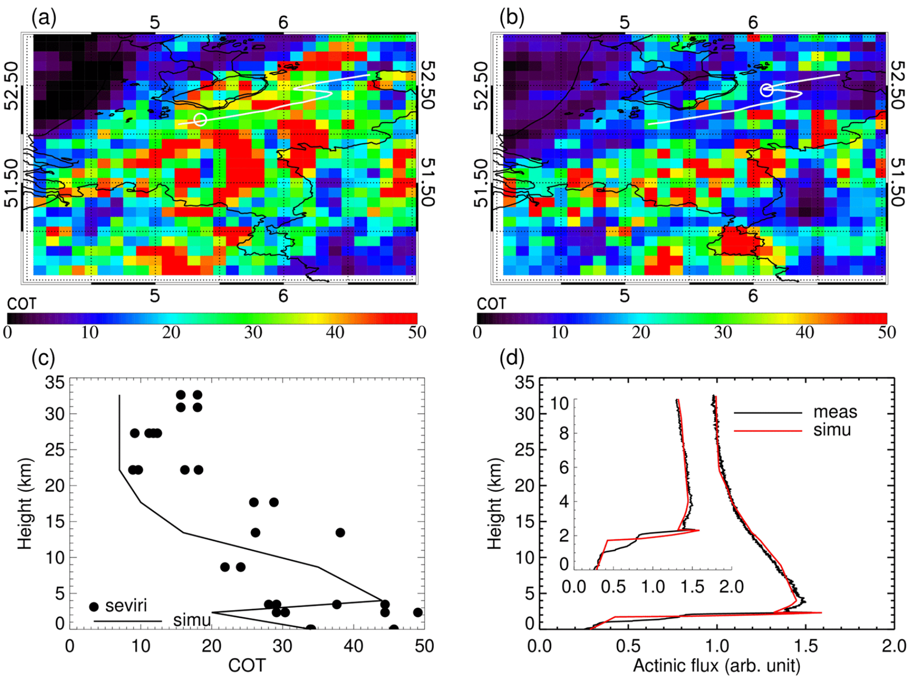

Figure 11. Same as Fig. ~~7~~ 9 but for 22 June 2006.

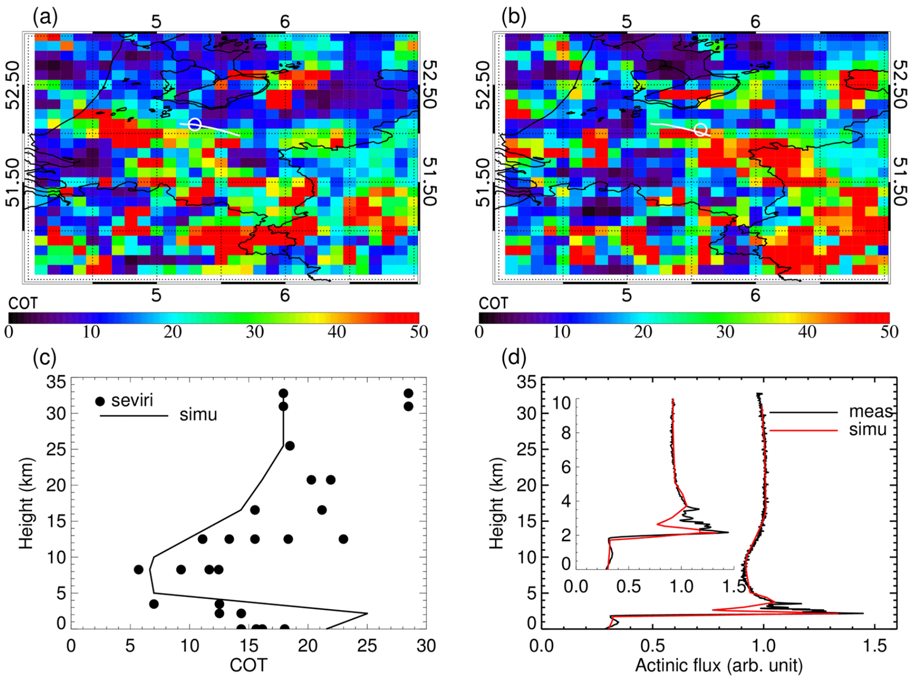

Figure 12. Same as Fig. ~~7~~ 9 but for 10 August 2006.

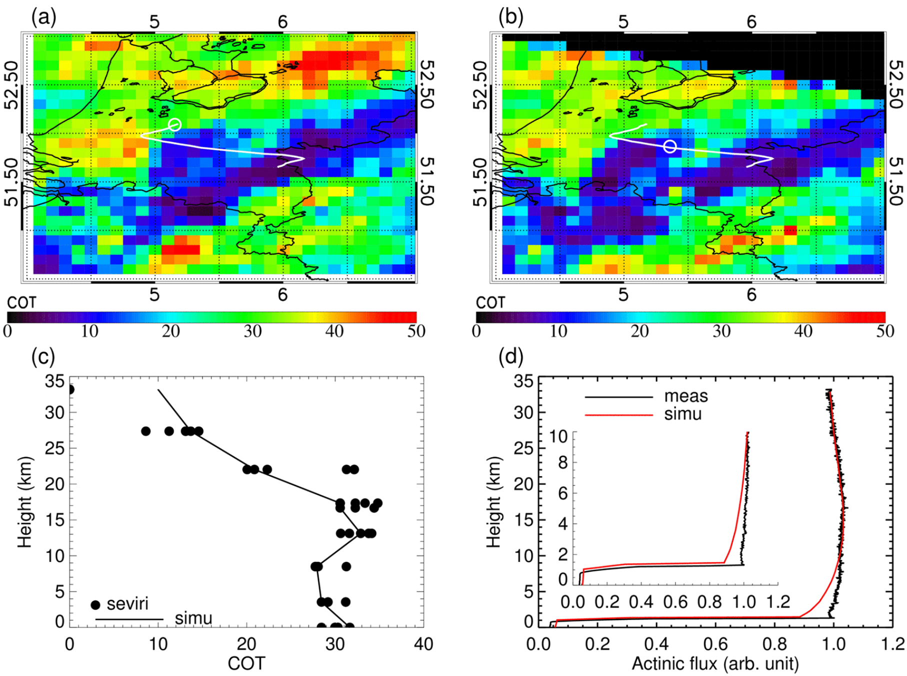

Figure 13. Same as Fig. ~~7~~ 9 but for 21 December 2006. **(b)** The SEVIRI image was acquired at 12:45 UTC instead of 13:00 UTC.

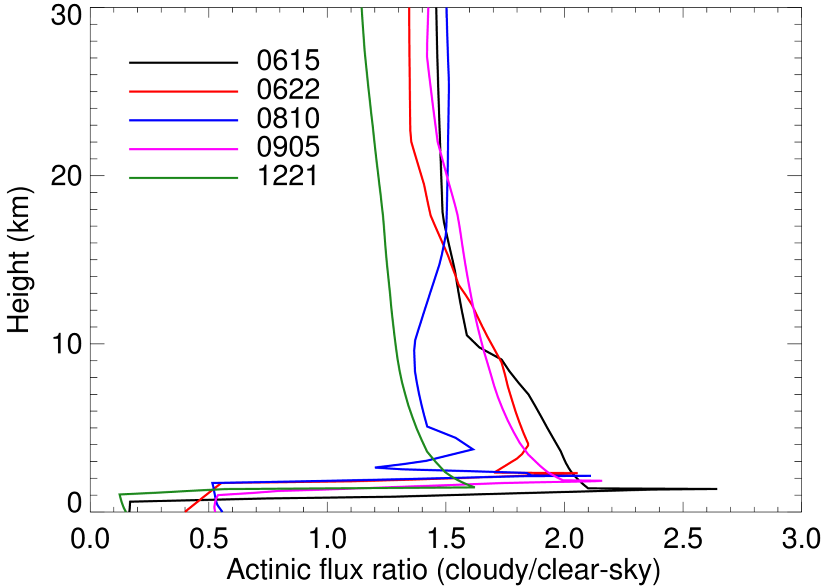

Figure 14. Simulated actinic flux ratio (cloudy/clear-sky) for the cloudy cases in Figs. 9-13.